REVIEWS OF TOPICAL PROBLEMS

Intense ion beams for generating extreme states of matter

V E Fortov, D H H Hoffmann, B Yu Sharkov

Contents

Abstract. **This paper reviews the basic ideas as well as the latest experimental results obtained in the rapidly emerging field that studies macroscopic thermodynamic parameters and collective phenomena occurring due to exposure of matter to an intense ion beam. Beams of accelerated heavy ions as a tool to produce extreme states of matter under reproducible experimental conditions have attracted the attention of scientists from around the world. This is largely due to the fact that an ion beam releases its energy into the volume of matter. Importantly, relativistic colliders, being unique tools for probing extreme states of matter, have opened up new possibilities for producing various states of matter, including those exhibiting exotic sets of thermodynamic parameters. The problems addressed by experiments in the field are of fundamental nature and deal with equations of states of supercompressed matter, plasma phase transitions, critical points of metals, anomalous conductivity, noncongruent phase transformations, and atomic physics with strong interparticle interactions.**

V E Fortov Institute of Thermophysics of Extreme States, Joint Institute for High Temperatures, Russian Academy of Sciences,
ul. Izhorskaya 13/19, 125412 Moscow, Russian Federation
Tel. (7-495) 484 23 00, (7-495) 483 23 14. Fax (7-495) 485 79 90
E-mail: fortov@ras.ru
D H H Hoffmann Institut für Kernphysik,
Schlossgartenstr. 9, D-64289 Darmstadt, Deutschland
Tel. +49-6159-71-2664. Fax +49-6159-71-2888
E-mail: D.Hoffmann@gsi.de
B Yu Sharkov Russian Federation State Scientific Center
'A I Alikhanov Institute of Theoretical and Experimental Physics',
ul. B. Cheremushkinskaya 25, 117218 Moscow, Russian Federation
Tel. (7-495) 123 02 88, (7-495) 123 80 93. Fax (7-495) 123 30 28
E-mail: boris.sharkov@itep.ru

1. Introduction

Increasingly more attention has recently been paid to states of matter with high energy densities responsible for gaining high pressures and temperatures. In the phase diagram [1 – 3], these states lie in a region between the low-temperature condensed state and high-temperature plasma (Fig. 1). This region is characterized by densities ranging from solid phase density to values 100 times higher and temperatures from 0.1 to 100 eV, at which matter takes the form of a nonideal plasma with degenerate electrons and strong interparticle interactions.

Two reasons are mainly responsible for current interest in extreme states of matter.

Firstly, studies of plasma with strong interparticle interactions extend the basic knowledge of nature because such plasma is the most widespread substance in the universe where astrophysical objects consist of strongly ionized high-density matter accounting for almost 98% of its total amount (except 'dark matter'). Moreover, much interest in superdense states of matter is stirred up by some challenging problems of modern planetary geophysics, such as determining the parameters of exoplanets (e.g., Jupiter's twin and exoplanets around Mu star of the Arae constellation), the exploration of Sun-orbiting planets (in particular, finding equations of state for ice on Neptune and Uranus and iron in the Earth's core), and investigations into hydrogen metallization, which are of importance for under-
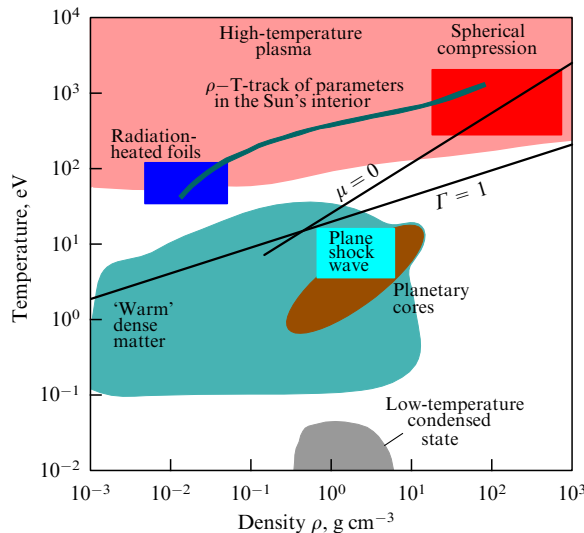
Figure 1. Phase diagram of matter [9]; μ is the chemical potential, and Γ is the parameter of nonideal plasma.

standing the structure of the giant planets Jupiter and Saturn.

Secondly, the studies currently underway are generally of great importance for such fields as the atomic power engineering, controlled nuclear fusion (CNF), the defense complex, the safety of nuclear reactors, the synthesis of superstrength materials, nuclear materials and technology, industrial plasma technologies, and medicine.

Plasma is known to acquire simple physical properties in two limiting cases, either at ultrahigh temperatures or at superhigh pressures. Interparticle interactions are rather weak at high temperatures and low matter densities, so that the Debye – Hückel quasi-ideal gas model is applicable in this case. In the second case, when internal atomic energy levels are compressed, it is possible to utilize the Thomas – Fermi theoretical model [1, 2, 4].

For a relatively cold high-density nonideal plasma, the ratio of Coulomb interparticle interaction energy to thermal energy exceeds unity, $\Gamma \geqslant 1$. Ions in such a plasma strongly interact with one another, while electrons are partly degenerate: $n_e \lambda_e^3 \sim 1$ (where $\lambda_e = [2\pi\hbar^2/(mkT)]^{1/2}$ is the de Broglie electron wavelength). This plasma is difficult to describe in theoretical terms because the electron system statistics are intermediate between Boltzmann and Fermi statistics.

This means that theoretical models in the region of interest in the phase diagram are near the applicability limit and their experimental verification is mandatory.

A key experimental problem is the laboratory generation of the states of matter with accurately measurable thermo-dynamic parameters. Recent progress in the enhancement of energy, power, and brightness of charged particle beams, lasers, and Z-pinch generators opens up new prospects for the creation of matter with an extremely high specific energy density under laboratory conditions. The new generation of experimental facilities ('drivers') makes it possible to reach a level of energy density in matter in excess of 10^{11} J m^{-3} and as a consequence to raise temperature and pressure up to 10^4 K and 1 Mbar, respectively. Such temperatures and pressures occur in shock-wave experiments with chemical explosives, in underground nuclear tests [5 – 9], and in the stars and cores of giant planets. In other words, new experimental facilities now

provide new opportunities for the laboratory exploration of physical phenomena commensurable with astrophysical objects in scale and for the generation of macroscopic amounts of matter possessing extreme thermodynamic parameters. It is noteworthy that the extreme state of matter achieved in the laboratory corresponds to that of the Universe within the first second after the Big Bang [2].

The majority of experiments are designed to resolve fundamental problems, viz. derivation of the equation of state for supercompressed matter, studies of plasma phase transitions, critical points of metals, anomalous conductivity and noncongruent phase transformations, and investigations into atomic physics phenomena with strong interparticle interactions [2]. Revolutionary developments in computing facilities that parallel the creation of high-power generators have given an incentive to computer simulation of compli-cated nonlinear dynamic processes and collective processes inherent in laboratory plasma under extreme conditions (including hydrodynamic motion which otherwise exists on a huge scale only in the Universe) [3].

Relativistic colliders of heavy ions are a special type of high-power energy sources (drivers). Big colliders operated in different countries provide a major experimental tool for nuclear physics, the physics of elementary particles, quantum chromodynamics, and the physics of superdense nuclear matter [10], i.e., for disciplines at the forefront of modern natural science. In other words, they extend our under-standing of the fundamental physical properties of Nature. Research based on these facilities requires increasingly higher energies and phase densities of accelerated particle beams.

Accelerator science and engineering have a remarkable history, from the first cyclotron with a proton energy of 1.2 MeV created by E Lawrence in 1932 to the Large Hadron Collider (LHC) with an energy of 7×10^6 MeV, now under construction at CERN. Between these two events, hundreds of various accelerators were put into operation around the world. These giant electrotechnical systems are the products of the highest technical achievements, accounting for the high degree of their reliability.

Among the experiments designed to be conducted with LHC is the collision of two proton beams with an energy of 7 TeV, to be followed by the observation of collisions between highly ionized lead ions Pb^{82+} with an energy up to 177 GeV per nucleon. The Relativistic Heavy Ion Collider (RHIC), in which the energy of colliding gold ions is as high as 500 GeV per nucleon in the center-of-mass system, was commissioned at the Brookhaven National Laboratory, USA at the turn of the 21th century. The cost of construction of the two most powerful relativistic hadron collider facilities (LHC and RHIC) amounts to a few billion dollars each, which is almost beyond the financial resources of the world's richest country and the international community like the European Union [11]. Research programs elaborated for these facilities include experimental studies of basic problems of high-energy physics covering hadron collisions accompanied by the synthesis of superdense nuclear matter, so-called quark – gluon matter. CERN and Brookhaven colliders have been used to carry out unique experiments that have resulted in the generation of a superextreme barion state of matter with a density of $\sim 10^{15}$ g cm^{-3} and temperature ~ 200 MeV in individual events of collisions between copper (Cu−Cu) and gold (Au−Au) heavy ions [12]. According to a modern concept, such was the state of matter in the Universe within the first microseconds after the Big Bang, and so it remains in certain

astrophysical objects like neutron stars and black holes. No wonder these experiments gave rise to speculation about their safety; it was argued that the creation of a black hole in the laboratory would be the end (!) of our civilization and the planet Earth itself. It is worth noting that numerical experiments in this field (so-called lattice studies) are carried out with the use of the world's most powerful supercomputers and seven- or higher-dimensional mathematical models.

It is of primary importance in the context of this paper that all these experiments have the objective of obtaining particle beams with ultrarelativistic energies and studying individual hadron–hadron collision events. Hence, a major characteristic of a collider from the standpoint of elementary particle physics is luminosity L expressed as the number of colliding particles per square cantimeter and second, thus determining the rate of collecting statistics [13]. (Projected LHC luminosity L amounts to appr. 10^{34} cm^{-2} s^{-1}.) The effects of collective interaction between the hadron beam and the targets are regarded as side ones and adverse.

In the general case, however, the loss of energy by a fast charged particle in a substance is due not only to elastic and inelastic nuclear processes, but also to its Coulomb interaction with target atoms. Moreover, cross sections of Coulomb interaction at small energies (below 500 MeV per nucleon) are many orders of magnitude larger than nuclear cross sections: $\sigma_c \sim 10^6 \sigma_n$. Hence, another reasonable (and natural) application of intense high-power charged particle beams may be to sharply change the thermodynamic parameters of the target material onto which the beam is focused by virtue of Coulomb heating due to the transfer of its kinetic energy to macroscopic volumes of the target material.

Certainly, the states of matter generated in this process are much 'less extreme' than those resulting from nucleus–nucleus collisions. Nevertheless, they are of great interest for the modern physics of nonideal plasma and its thermonuclear and astrophysical applications owing to their characteristic megabar pressures.

It is worthwhile to emphasize that the parameters of modern colliders make them equally suitable for the generation of dense nonideal plasma. Specifically, it was noticed that the total kinetic energy of accelerated and accumulated ion beams in modern colliders is already as high as a few hundred kilojoules. The total proton beam energy of the CERN LHC will be ~ 300 MJ. Evidently, the concentration of this huge energy in a small volume of matter within a very short period opens up inviting prospects for the generation of its extreme state in macroscopic volumes [14].

It is these properties of intense ion beams that underlie the proposal (dating back to the early 1980s) to use high-power heavy ion colliders for inertial confinement fusion [15] (see Section 7).

In this review, attention is focused on the results of research into the macroscopic thermodynamic parameters of matter and the collective phenomena arising in it under the effect of an intense ion beam. Today, interactions between fast heavy ions and matter in different states (including extreme thermodynamic ones) are the topical issues of experimental and theoretical studies. They are attracting the attention of scientists working in Russia, Germany, France, the UK, the USA, and Japan. The total funds allocated annually by governmental agencies throughout the world to support these projects amount to roughly 100 mln dollars, enabling the researchers to use up-to-date colliders [16, 17].

Thus, the objective of this paper is to review scientific ideas and consider new experimental results obtained in this rapidly developing field of physical knowledge.

2. High-power heavy ion colliders

Topical scientific problems facing the physics of elementary particles, on the one hand, and applied problems related to the generation of extreme states in macroscopic volumes of matter, on the other hand, put in different claims to the parameters of colliders needed to resolve them. The solution of scientific problems requires maximum energies of accelerated particles and collider luminosities, whereas relatively small energies (5–50 GeV per nucleus) and the highest intensity of maximally heavy particles are sufficient for practical purposes. Several modern colliders combine the two above regimes, which enables accelerator laboratories based on them to realize scientific projects comprising experimental studies of both types. Macroscopic heating of matter is achieved with a collider beam whose assemblage of parameters ensures a specific energy deposition, E_s, above the threshold level: $E_s \geqslant 1$ kJ g^{-1}, sufficient to evaporate and ionize the majority of target materials (see Section 3). Colliders aptly combining the above regimes are exemplified by world-renowned heavy ion facilities, SIS-18[1] at Gesellschaft für Schwerionenforschung (GSI), Darmstadt, Germany [16, 18] and the TeraWatt Accumulator (TWAC) at the Institute of Theoretical and Experimental Physics (ITEP), Moscow [17].

At the same time, a number of concrete experiments aimed at the elucidation of the physical nature of interactions between intense ion beams and matter are being carried out using ion and even proton beams from low-power accelerators. By way of example, interesting results were obtained using the U-400M cyclotron of the Joint Institute for Nuclear Research (JINR), Dubna; a collaboration of the University of Erlangen, Germany, and the Institute of Nuclear Physics, University of Paris, Orsay, France, and the heavy ion linac at the Tokyo Institute of Technology, Japan etc. [15].

The most intense ion beams are produced with the GSI heavy ion synchrotron (Fig. 2). This accelerating complex comprises the Universal Linear Accelerator (UNILAC) serving as a linear injector and two storage rings: the SIS-18 synchrotron with a magnetic rigidity of 18 T m and the Experimental Storage Ring (ESR). The flexible application of various ion sources makes it possible to use ions in a wide range of atomic masses — from carbon to uranium.

Focused beams of ions with energies of 200–300 MeV per nucleon, extracted from the SIS-18 ring, are employed to generate states of matter with high energy densities. The presently available intensity of uranium ion beams amounts to $\sim 5 \times 10^9$ (number of particles per pulse); this ensures specific energy deposition ~ 1 kJ g^{-1} sufficient to heat a tungsten target up to 4000 °C. Also actively utilized in experiments are ion beams with an energy of 3–10 MeV per nucleon from UNILAC; they interact with various types of plasma targets, viz. discharge in a gas, laser plasma, and the plasma of explosive generators (see Section 5).

Modernization of systems entering into the accelerating complex is currently underway not only to enhance ion beam intensity in SIS-18 to the maximum possible value in terms of

---

[1] SIS — abbreviation from the German Schwerionen Synchrotron (Heavy Ion Synchrotron).
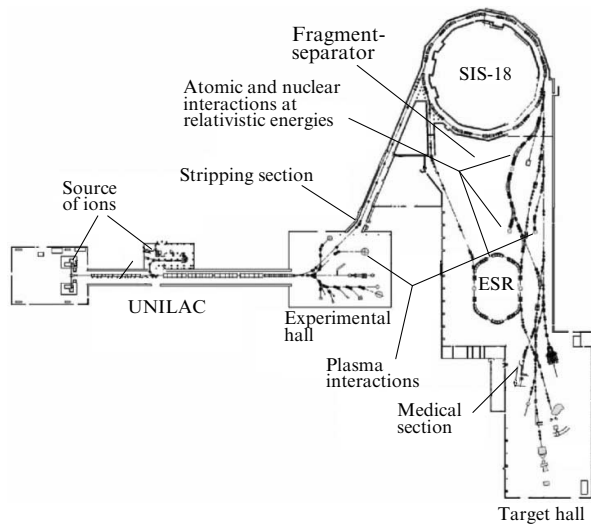
Figure 2. Schematics of GSI accelerating complex in Darmstadt, Germany [18].

Figure 3. Schematics of TeraWatt Accumulator (TWAC) at ITEP, Moscow.

spatial charge effect ($\sim 10^{10}$ particles per pulse for uranium ions) and to reduce the duration of pulse on a target to $50 - 100$ ns by means of time-dependent compression of the beam under the effect of a high-frequency (HF) field.

In 2007, construction of a new accelerating complex SIS-100/300 commenced at GSI in the framework of the Facility for Antiproton and Ion Research (FAIR) international project [19]. This complex will be using SIS-18 in service today as the injector. The new facility will have parameters sufficient to reach an energy deposition in excess of 100 kJ g^{-1}. Studies in high energy density physics (HEDP) are an important component of the research program being elaborated for the new collider. The distinctive feature of the new facility will be the possibility to combine both the effects of high-power heavy ion pulses and high-power laser pulses on a substance inside a single experimental chamber. A neodymium glass petawatt high-energy laser for heavy ion experiments (PHELIX) is being developed for the purpose [20].

The heavy ion storage-accelerator complex — TeraWatt Accumulator (TWAC) — was commissioned at ITEP in 2003 (TWAC-ITEP project) [17, 21] (Fig. 3). Physical start-up of the new facility was successfully performed to confirm operability of the master scheme and all its key elements and systems. The work initiated in 1997 had the purpose of radically modifying the ITEP U-10 synchrotron, small UK auxiliary storage ring, I-3 heavy ion injector, and laser source of ions. The principal goal of the project was to achieve a terawatt power level (100 kJ 100 ns^{-1}) of accelerated and accumulated ion beams with an intermediate mass (atomic number $A \sim 60$).

By now, the world's first sophisticated technological chain for the acceleration and storage of intense heavy ion beams has been realized to support a series of basic and applied research in the following fields:
 • physics of high energy density (HEDP) in matter;
 • fundamental relativistic nuclear physics;
 • the nuclear fuel cycle;
 • medical physics;
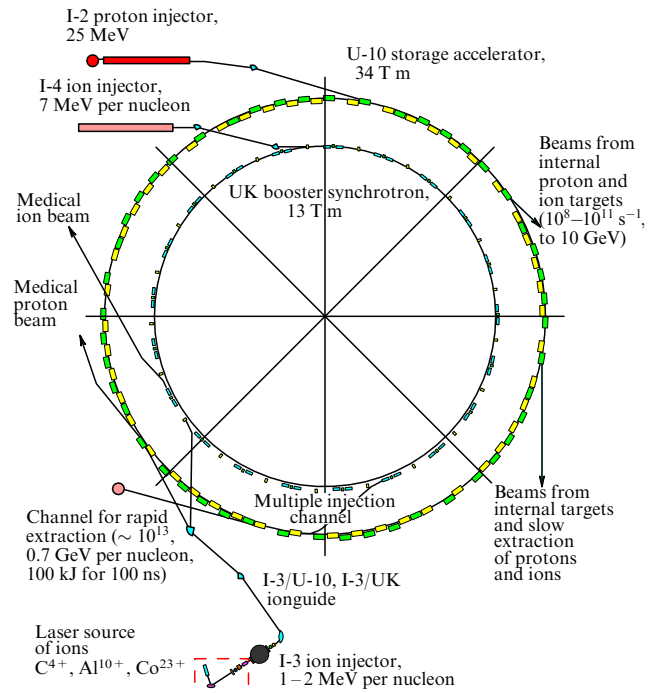 • the physics of high-current ion beams and charged particle accelerators.

The new facility is capable of accelerating ions to an energy of 4.3 GeV per nucleon for experiments in relativistic nuclear physics. Also, it accumulates heavy ions with an energy of hundreds of megaelectron-volts per nucleon for subsequent compression of the accumulated beam to the terawatt power level and for HEDP experiments in matter. Today, the TWAC-ITEP storage accelerator facility comprises the 4 MeV I-3 ion injector, the UK booster synchrotron (700 MeV per nucleon), and the U-10 storage ring with systems for multiple non-Liouvillian injection of the ion beam, rapid extraction of the accumulated beam, and the beam transport channel directed toward an experimental target. The next stage of modification of the TWAC-ITEP accelerating complex scheduled for 2006 – 2009 envisages further improvement of its operational performance and extension of the range of experiments to be conducted on this facility, including physical studies with heavy ion beams at an energy deposition level of ~ 10 kJ g^{-1}. Thus, it is expected that new high-power heavy ion TWAC-ITEP and SIS-100 facilities will be used in the near future to increase the energy deposition of its present level by dozens of times, i.e., up to $\sim 10 - 100$ kJ g^{-1}.

3. Peculiarities of physical processes in ion – matter interactions

In the accelerated particle energy range of interest ($\leqslant 500$ MeV per nucleon), heavy ions transfer their kinetic energy to the target substance in the bulk along the path of the particles undergoing deceleration. This process is accompanied by energy exchange during Coulomb collisions with free and bound electrons and with ions of the stopping medium. Simultaneously, a charged ion beam has the important merit of a strictly linear direction of the particle's track and a pronounced energy release peak at its end (the so-called Bragg
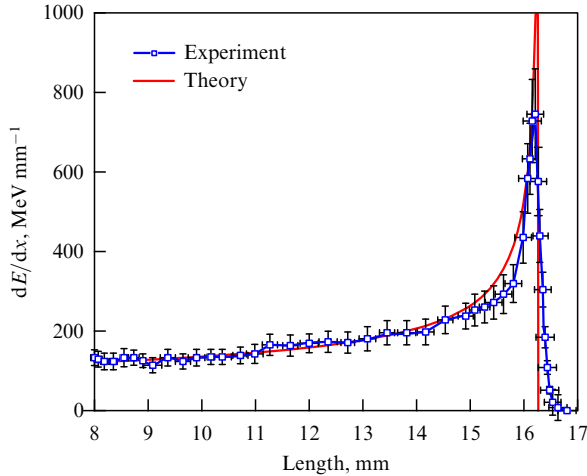
Figure 4. Experimental and theoretical energy release profiles of a beam of C^{6+} nuclei in a copper target [23]. The TRIM (transport of ions in matter) model was used in calculations.

Figure 5. Dependence of the range of ions with various masses on particle energy in cold matter.

Figure 6. Dependence of the temperature of various substances on specific energy deposition of the ion beam [24].

peak) [22, 23] (Fig. 4). Such a property is lacking in any other ionizing radiation.

Thus, intense beams of high-energy heavy ions have an important advantage with respect to their capability of generating extreme states of matter under reproducible experimental conditions. Indeed, selection of particles' energy, mass, and charge, as well as target geometry, permits obtaining a desired energy release profile and ensuring beam energy absorption efficiency up to ~ 100%. As shown below (Section 4.2), it is possible, in principle, to realize a uniform distribution of thermodynamic parameters of matter being heated along most of the track of the ion stopping range. Volumes of several cubic millimeters are typically heated during a rather long time (10 – 100 ns), thus facilitating the performance of reliable experiments.

The ability of heavy ions to heat matter [16, 18, 24] is characterized by the specific energy deposition:

$$E_s = 1.6 \times 10^{-19} \frac{N_i \, dE/(\rho \, dx)}{\pi R_0^2} \; [\text{J g}^{-1}], \qquad (1)$$

where ρ is the density of the matter, N_i is the number of particles in the beam, R_0 is the radius of the beam focal spot at the target, and $dE/(\rho \, dx)$ are the specific stopping losses of ions in the target material.

It appears that beam intensity N_i must be increased if high E_s values are to be achieved; simultaneously, the beam focal spot needs to be diminished. Specific ion energy losses determine the ion stopping range in a substance, $l_i \sim E^\alpha$ ($\alpha = 1.5$). It will be shown in Section 4 that these losses strongly depend on the ion charge and stopping medium properties.

Figure 5 illustrates the dependence of the range of ions with various masses on the particle energy in cold matter. Evidently, a lead ion releases 1000 times more energy than a proton within an equal total ion range. Therefore, the intensity of heavy ion beams may be three orders of magnitude lower than that of a proton beam to release the same quantity of energy in 1 g of matter. This means that high-energy heavy ions with large $dE/(\rho \, dx)$ ensure a given level of specific energy deposition E_s [J g^{-1}] at a smaller beam current.
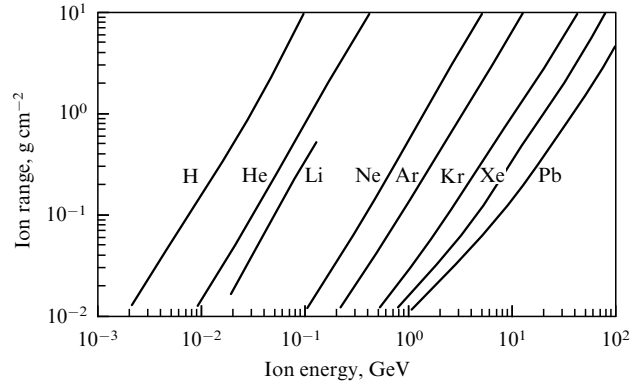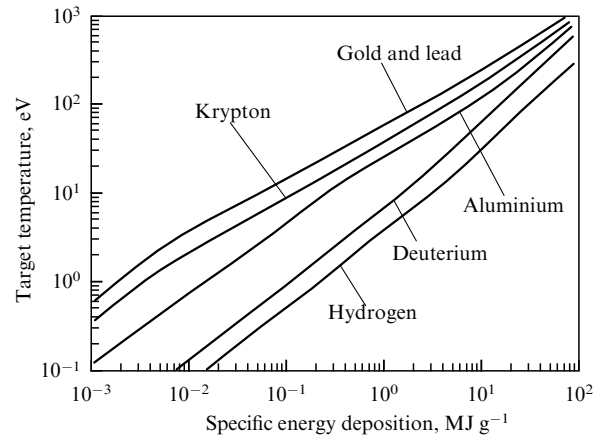
Substance heated by an ion beam is set in hydrodynamic motion under the effect of pressure forces. Strictly speaking, heating is quasi-isochoric if the duration τ_b of the heating beam is smaller than the characteristic time $\tau_h \sim R_0/c_s$ (where c_s is the speed of sound) of the substance expansion. Figure 6 shows scale relations between the temperature of various substances and the specific energy deposition of the beam [24].

For comparable times, $\tau_b \leqslant \tau_h$, the parameter is given by the specific power P_s [W g^{-1}]. The relation between temperature T, specific power input P_s, and focal spot radius R_0 in a wide range of ion energies (50 – 1000 MeV a.m.u.$^{-1}$) is fairly well approximated by the formula [3, 24]

$$T = f(P_s) = 60 \left(P_s \, [\text{TW g}^{-1}] \, R_0 \, [\text{cm}] \right)^{1/2} \; [\text{eV}]. \qquad (2)$$

It follows from the analysis that an ion pulse containing ~ 10^{12} heavy ions is needed to achieve specific energy deposition of 10 – 100 kJ g^{-1} and corresponding temperature of 10 – 100 eV at normal density $\rho = \rho_n$ and pressure $P \geqslant 1$ Mbar. Such pressure and temperature levels are realized in shock-wave experiments with chemical explosives and in underground nuclear tests (see Section 4.1). It is clear, however, that modern colliders make it possible to run experiments in reproducible laboratory conditions with a high pulse repetition rate unattainable in explosion experi-

Table 1.

Driver \ Parameters	Angara-5 accelerator	Iskra-5 accelerator	Chemical explosives	Nuclear explosives	TWAC-ITEP
Energy, kJ	$100-300$	30	$4 \times 10^4 - 4 \times 10^5$	$10^5 - 10^6$	100
Specific energy, MJ g^{-1}	1		0.01	$1-10$	0.1
Power, TW	10	$5-100$	1	1000	1
Specific power, TW g^{-1}	$1-10$		0.01	10	$1-10$
Flux density, TW cm^{-2}	5	$100-1000$		100	100
Pulse length, ns	20	0.5	1000	1000	100
Temperature, eV	100	170	$1-10$	$100-1000$	$1-40$
Implosion velocity, cm s^{-1}	10^6	3×10^7	$(1-2) \times 10^6$	$(2-3) \times 10^6$	$(1-2) \times 10^6$
Pressure, Mbar	3	$1-10$	10	$10-100$	$0.1-50$

ments. The sum total of physical states of matter that can be produced using intense heavy ion beams is presented in Table 1 in comparison with extreme states of matter generated by other drivers [1].

Thus, relativistic colliders of heavy ions took up a prominent place among high-power energy sources — drivers, which are employed to explore extreme states of matter — due to peculiar features of physical processes associated with the stopping of intense heavy ions in a substance. The objective of experiments with heavy ion beams is to study equations of state, plasma phase transitions, critical points of metals, conductivity, noncongruent phase transformations, and atomic physics phenomena with strong interparticle interactions.

HEDP investigations using heavy ion beams have important practical implications for inertial confinement controlled fusion, nuclear reactor safety, materials science, plasma technologies, astrophysics, and planetary geophysics.

4. Generation of extreme states of matter by intense ion beams

4.1 Shockless generation of high-energy states
The volumetric character of ion beam energy release into matter creates prerequisites for the generation of high-entropy states of matter without employing the regime of shock-wave compression. The diagram plotted on the pressure–entropy coordinates (Fig. 7) shows that states of matter with high energy density occupy a vast area [25] encompassing regions of hot compressed ionized substance, nonideal plasma, heated expanding liquid, and quasi-ideal plasma.

The shock-wave compression technique enables investigations to be carried out in a relatively narrow region of the phase diagram along the Hugoniot adiabat for solid and porous specimens [26]. In this case, reliable experimental data
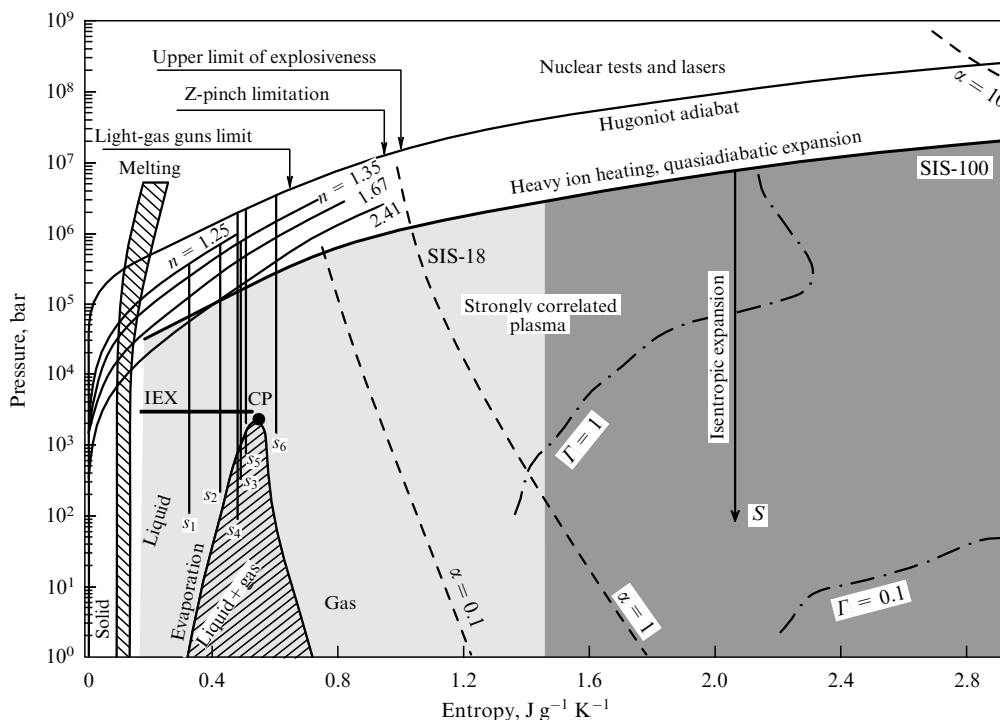

Figure 7. States-of-matter diagram plotted on the pressure–entropy coordinates: IEX — ion expansion, CP — critical point, and n — porosity.

can be obtained if rigorous requirements are imposed upon the quality of shock-wave fronts, reproducibility of driver characteristics, and so forth.

The available data on shock compressibility of solid specimens along the Hugoniot adiabat cover a nine-order-of-magnitude pressure range. Multimegabar pressures have been achieved in explosion experiments for certain metals [5, 6]. Higher pressure levels have been obtained in spherical cumulative systems [1, 2] and in underground nuclear tests [8, 9]. By way of example, a pressure of up to approximately 4 Gbar was documented in underground nuclear tests. Modern high-power lasers make it possible to reach a 10-Mbar pressure [27, 28].

It should be emphasized that typical shock-wave methods can only be used to study the so-called caloric properties of matter — that is, the relationship between its internal energy, pressure, and volume in the form $E = E(P, V)$. However, the function $E = E(P, V)$ does not close the equations of thermodynamics; therefore, temperature or entropy needs to be measured for calculating the first and the second variables, such as heat capacity, speed of sound, and so forth [1, 2]. There are scarce data on the temperatures of shock-compressed metals along expansion isentropes. Meanwhile, the knowledge of temperature is indispensable for verifying the theoretical models. Of special interest in this context are the results of closed thermodynamic measurements taken by the 'exploding wire' technique at isobaric expansion of a heated substance [29]. It is in this way that the states of several liquid metals were measured near the critical point (see Fig. 7).

The majority of available data on metal properties, obtained by the isentropic expansion method, are distributed over the Hugoniot adiabat and supplemented by model-based estimates of critical point positions on the phase plane. For this reason, further studies are required to characterize the vast area beneath the shock adiabat in the phase diagram, which contains regions with critical points of metals and the nonideal plasma region ($\Gamma \geqslant 1$).

Intense beams of heavy ions make it possible to rapidly (compared to the characteristic time of hydrodynamic motion) heat a substance and then observe its expansion into the environment, i.e., to reach a high level of energy release and sequentially examine isentropic expansion. In such an experiment [16, 18, 25], the expanding heated material will pass through a number of new interesting states. For example, a heated metal of initially normal density will turn into an overheated liquid with a disordered ion component and degenerate electrons. In the course of isentropic expansion, a substance passes through the states of quasinonideal Boltzmann plasma and rarefied gas. As the expansion progresses, the degree of degeneracy decreases, thus leading to rearrangement of the energy spectra of ions and atoms, as well as partial recombination of the dense plasma. A disordered electron system facilitates metal–insulator phase transitions, while plasma near the critical point and the point of liquid–evaporated phase equilibrium becomes nonideal. When the isentrope enters the two-phase liquid–vapor region, the gaseous phase begins to condense. At higher energy deposition levels, isentropic expansion may be accompanied by even more exotic effects with marked variations in the degree α of plasma ionization and nonideality parameter Γ. The thermodynamic parameters of a substance in one experiment may vary considerably — that is, over six orders of magnitude in terms of pressure and four orders of magnitude in terms of density.

The phase diagram in Fig. 7 exhibits regions corresponding to the parameters attainable with heavy ion colliders SIS-18 and SIS-100. The former facility generates a heating pulse of uranium ions containing $\sim 10^{10}$ particles; its duration equals ~ 100 ns at an ion energy of 300 MeV per nucleon. Focusing such a pulse onto the target ensures an energy release level of about 1 kJ g^{-1}. Future plans for GSI include increasing the beam intensity, taking the level of energy deposition to $10-20$ kJ g^{-1}. The TWAC-ITEP facility commissioned in 2003 is designed to produce specific energy release of $\sim 10-20$ kJ g^{-1} when focusing the beam of copper or cobalt ions with energies of up to 700 MeV per nucleon on the target. The construction of the new SIS-100/300 collider was initiated at GSI in 2007; it is expected to ensure specific energy deposition of ~ 100 kJ g^{-1}.

To conclude, the development of heavy ion drivers-colliders opens up new prospects for investigations into previously inaccessible regions of the phase diagram for substances with substantially different physical properties.

4.2 Quasi-isochoric heating

As shown in Section 3, specific energy deposition E_s, which can be determined experimentally to a high accuracy, is the main characteristic of volumetric energy release from a beam of ions with an energy $E \geqslant 10$ MeV per nucleon. When the substance density ρ_0 in a sample being heated remains unaltered, its post-irradiation thermodynamic parameters depend on ρ_0 and E_s. In other words, any measurable physical quantities are functions of such a well-defined thermodynamic state.

Reference [30] put forward a physical rationale for an impending experiment with ion beams of the collider SIS-100 being constructed in Darmstadt in the framework of the international FAIR program. The aim of this experiment is to study solid-state hydrogen at an energy deposition of 130 kJ g^{-1} provided by a uranium ion beam with an energy of 200 MeV per nucleon and intensity 8×10^{10} particles per pulse focused on a spot with radius $r_b = 350$ μm (rms value). In accordance with the equations of state from the SESAME[2] tables, this situation corresponds to a temperature of 0.6 eV, i.e., to the 'warm dense matter' regime at which the entire beam energy is transferred to the inner energy of the substance.

The choice of material for a target is dictated by the scope of the diagnostic method based on recording spectral and angular distributions of X-ray quanta scattered by the heated sample substance (X-ray Thomson scattering method) [31]. Such X-ray time-resolved illumination is expected to be provided by the PHELIX petawatt laser being constructed at GSI, Darmstadt. However, the choice of target materials at X-ray photon energies in the range of $\sim 1-3$ keV is restricted to elements with small Z. It is more preferable to have specimens with uniform bulk density distribution for the diagnostics of the states of substance and data interpretation. The simplest target for conducting a quasi-isochoric experiment is a cylinder of frozen hydrogen with radius $R_h \geqslant r_b$ (Fig. 8). For a rectangular intensity distribution across the ion beam section, density along the cylinder axis remains constant until the unloading wave reaches the axis. However, for a real beam with a Gaussian intensity distribu-

---

[2] SESAME (*S*oftware *E*nvironment for the *S*imulation of *A*daptive *M*odular Syst*e*ms) — standardized computer library of tables containing the thermodynamic parameters of materials.
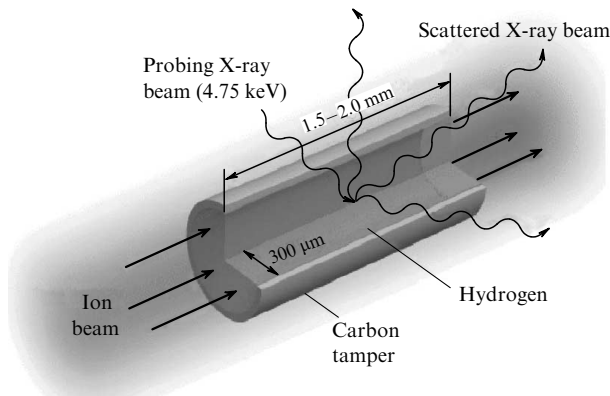
Figure 8. Schematics of a quasi-isochoric hydrogen heating experiment [30].

Figure 9. Evolution of mean hydrogen density over the target cross section [30].

Figure 10. Structure of a multilayer cylindrical target for the LAPLAS experiment [40].

tion over the cross section, at which the second derivative of the pressure with respect to the radius differs from zero, the density begins to drop before the unloading wave arrives at the target axis.

Such an effect of hydrodynamic unloading of the heated target portion can be compensated for by using an inert tamper bounding frozen hydrogen. To ensure the required 'confinement' of a heated small-Z material as being transparent to X-ray quanta, the tamper is also heated by the peripheral part of the ion beam. In this case, the heated layer of the tamper creates confining counterpressure for the principal target material. Evidently, a material with an enhanced sublimation energy is most suitable for manufacturing tamper since it delays the onset of hydrodynamic expansion of the tamper itself.

Numerical simulation based on the two-dimensional hydrodynamic BIG-2 code [32] has shown that tamper density should be lower than graphite density. Therefore, we chose a plastic material of density 1.5 g cm^{-3} under normal conditions. In the beginning, hydrogen density was decreasing due to the Gaussian profile of the ion beam. Pressure inside the tamper material became higher than the hydrogen pressure, which caused the tamper to move inwards, thus creating a weak shock wave. Thereafter, when tamper density decreased, the pressure equalized, and the hydrogen – tamper interface stood motionless. Still later, it returned to the initial position as hydrogen pressure increased. Calculations indicated that target density became almost uniform along the target radius, when the effect of the ion beam was no longer apparent.

Figure 9 displays the evolution of mean hydrogen density over the target cross section. The tamper thickness is chosen depending on the desired result: either minimal (10–15%) density variations in the course of heating (a tamper with thickness 50 μm) or hydrogen density at the end of the heating pulse equal to its initial value of 0.1 g cm^{-1} (a tamper with thickness 60 μm). Thus, it has been shown that an ion beam can ensure quasi-isochoric heating of a substance at a given set of initial parameters.

4.3 Cylindrical implosion to produce highly compressed matter

Great efforts of computing theoretical groups are made to study cylindrical implosion of substance under the effect of intense heavy ion beams. Interest in this phenomenon is due to the development of inertial confinement fusion based on
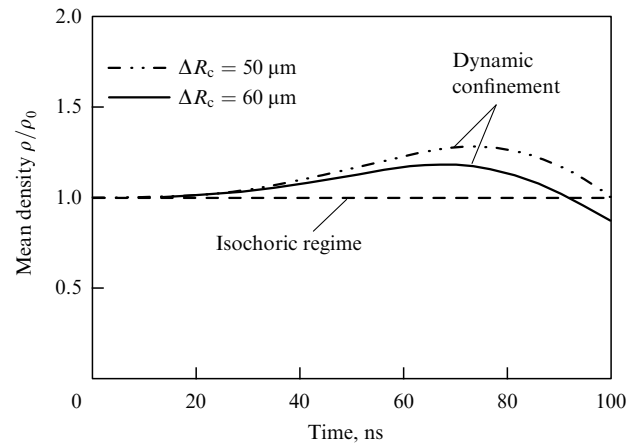
the heavy ion driver-collider. The specificity of the modern approach to the problem arises from the fact that physical path lengths of ions having an energy of hundreds of megaelectron-volts per nucleon do not exceed a few millimeters. This makes the practical realization of spherical implosion difficult and energetically inefficient (see Section 7).

As a rule, targets consist of several cylindrical layers with different initial density (Fig. 10).

Their central core is composed of a substance that needs to be compressed to the highest possible final density, e.g., an equimolar DT mixture. The ion-energy absorbing layer (absorber) is exposed to a 'tubular' beam of a special shape and with an annular cross section. The generation of thus-shaped ion beams by their rotation in an HF field during ion transport from the accelerator to the target was proposed in Ref. [33]. Some computation-theoretical papers report on searching optimal conditions for homogeneous hydrodynamic response of the absorbing material to the energy released by such rapidly revolving beams [34, 35].

Special attention is given to obtaining such a combination of heating pulse parameters of the ion beam, geometric sizes of target layers, and their initial densities that would ensure fuel compression on the cylinder axis in a near-adiabatic regime [36].

The possibility of achieving maximum compression ratios for various porous materials by means of cylindrical implosion was considered in Ref. [37]. A beam of ^{60}Co ions with an energy of 40 GeV, a total energy of 60 kJ, and a duration of 100 ns conforming to the parameters of the TWAC-ITEP system under construction was chosen as the heating beam. It was utilized to heat a 180-μm-thick

cylindrical layer of gold with normal initial density; its inward expansion caused implosion of the substance in the target's central region. Maximum compression ratio $\rho_{max}/\rho_0 \sim 35$ was achieved for the porous material having initial density 0.975 g cm^{-3}. For substances of normal initial density, viz. carbon (0.975 g cm^{-3}), aluminium (2.7 g cm^{-3}), iron (7.8 g cm^{-3}), and gold (19.5 g cm^{-3}), the degree of compression was as high as $\rho_{max}/\rho_0 \sim 3-5$.

For cylindrical implosion of DT gas with an initial density of 0.2 g cm^{-3} [37], the fuel is compressed to ~ 20 g cm^{-3} and heated to 150 eV, which leads to the generation of $\sim 10^5$ thermonuclear neutrons per pulse.

Specific conditions of cylindrical implosion in the event of strong fuel magnetization by the imposition of a ~ 30 T longitudinal magnetic field along the axis of the cylindrical target were explored in Refs [36, 38, 39]. The magnetic field suppressed electron heat conductivity in the radial direction and significantly increased the thermonuclear yield of the targets.

4.4 Quasi-isentropic regime

Cylindrical implosion will also be applied in experiments on the generation of superdense states of matter using ion beams of the SIS-300 facility under construction at GSI. One of the three experimental programs elaborated by the Physics of Plasma Collaboration in the framework of the international FAIR project is the LAPLACE (*La*boratory of *Pla*netary *Sc*iences) experiment [18, 40] aimed at the investigation of hydrogen metallization believed to occur in the internal layers of the giant planets Jupiter and Saturn.

A two-dimensional hydrodynamic code [32] was employed in a numerical study of the possibility of realizing a quasi-isentropic regime of compression by a heavy ion beam in order to observe metallization of hydrogen predicted by Wigner and Hugoniot in 1935. The numerical experiment made use of a 3-mm-long multilayer cylindrical target with an outer radius of 3 mm (see Fig. 8), with the radius of the inner cylinder of solid frozen hydrogen being 0.5 mm. A uranium ion beam with an energy of 400 MeV per nucleon, intensity of 10^{12} ions per pulse, and pulse duration of 50 ns was directed from the butt end of the cylinder toward the target. An important feature was the annular cross section of the beam focused onto a ring with an outer radius of 2 mm and inner radius of 0.5 mm. The beam affected the cylindrical layer of lead but not hydrogen. Energy release along this layer was assumed to be homogeneous because the uranium ion range in lead was 4.25 mm for an ion energy of 400 MeV per nucleon and, as a result, the Bragg peak lay outside the target.

The experiment was designed to ensure generation of many sequential reverberating weak shock waves needed to compress hydrogen along the isentrope.

The two-dimensional hydrodynamic BIG-2 code [32] permits calculating hydrogen density distribution along the cylinder radius at different instants of time. The results indicate that the relatively slow adiabatic motion of the hydrogen–lead interface towards the cylinder axis causes a series of weak reflected shock waves between the interface and the axis; they create a state of matter meeting hydrogen metallization conditions. In accordance with the equation of state from a SESAME table, these conditions include pressure equaling 3 Mbar, density ~ 1 g cm^{-3}, and temperature $\geqslant 0.1$ eV [40]. Such parameters should remain stable for 160–200 ns, long enough to experimentally examine hydrogen conductivity under extreme conditions.

Similar computation-theoretical studies [41] were later performed for a different model of the hydrogen equation of state based on the semiempiric fluid variational theory (FVT) [42, 43]; this model takes into account molecular dissociation in neutral fluids. The FVT equation of state supplemented by the Padé approximation suggests higher hydrogen compressibility than the SESAME equation of state.

The experiment on the generation of 'reverberating' weak shock waves in matter using a heavy ion beam of the SIS-18 facility at GSI was practically realized in plane geometry [44]. Shock wave velocities (~ 300 m s^{-1}) measured by Toepler's schlieren method in a transparent substance proved to be in excellent agreement with the results of 2D numerical calculations [45].

5. Theoretical and experimental studies of energy release processes with heavy ions

Investigations into the physics of extreme states of matter induced by intense heavy ion beams have attracted heightened interest to new aspects of interactions between heavy ions and plasma, with its strong ionization and interparticle interactions. Earlier work in this area was dictated by the necessity to determine real ion ranges and energy release profiles in a dense plasma in inertial confinement fusion (ICF) experiments [46–48].

5.1 Ion stopping in an ideal plasma

To begin with, it needs to be emphasized that the stopping of an ion beam is due to the energy loss by single particles as they undergo Coulomb interactions with electrons and ions of the stopping medium, even in the event of maximum intensity of an ion beam focused on the target of an ICF driver-collider ($\sim 5 \times 10^{24}$ s^{-1} cm^{-2} for Bi ions with an energy of 10 GeV) [49].

The energy (or velocity) of incoming particles is the key parameter in the description of ion–matter interactions. In general, the total stopping power of the medium for a separate ion of the beam may be conveniently represented in the form of four terms:

$$S_b = -\frac{1}{\rho}\frac{dE}{dx} = S_{be} + S_{fe} + S_{fi} + S_{nu} , \qquad (3)$$

describing the contribution of bound and free electrons, free plasma ions, and 'bare' nuclei, respectively (ρ is the bulk density of the target). In the ion energy range of interest ($\sim 1-500$ MeV per nucleon), the contribution from nuclear interactions and the influence of free plasma ions are usually neglected.

The expression for the stopping power S_{be} of bound electrons in the general case (the Bohr–Bethe–Bloch formula) has the form [46, 47, 49]

$$-\frac{dE}{dx} = \frac{4\pi Z_{eff}^2 e^4 \rho}{mv^2}\frac{Z-y}{Am_A}\left(L_{be} - \ln(1-\beta^2) - \beta^2\right). \qquad (4)$$

Here, e and m are the electron charge and mass, respectively, Z_{eff} and v are the effective charge and velocity of an incoming ion, $\beta = v/c$ (where c is the speed of light), A, Z, and y are the mass, atomic number, and degree of ionization of medium atoms, $Z-y$ is the number of bound electrons per atom of the medium, m_A is the atomic mass unit, and L_{be} is the Coulomb logarithm for bound electrons without relativistic corrections

(excluded in order to further deal with nonrelativistic pulses and energies when writing it).

When $L_{be} \gg 1$, this quantity can be represented as

$$L_{be} = \ln \frac{p_{max}}{p_{min}} , \qquad (5)$$

where p_{max} and p_{min} are the maximum and minimum values of a momentum that can be transferred as a result of a collision between an ion and a field particle (in this case, with a bound electron).

The results of the Bohr–Bethe–Bloch approach were directly generalized to the case of a rarefied plasma [48–51] by the appraisal of the stopping power of continuous spectrum electrons using formulas from the theory of ideal plasma.

M Basko summarized the results of some theoretical studies and proposed the following algorithm to calculate S_{fe} [49]:

$$-\frac{dE}{dx} = \frac{4\pi Z_{eff}^2 e^4 \rho}{mv^2} \frac{yG(v/v_e)}{Am_A} \left[L_{fe} - \ln\left(1 - \beta^2\right) - \beta^2 \right], \quad (6)$$

where L_{fe} is the Coulomb logarithm for free electrons, and v_e is the velocity of the target's free electrons.

If the velocity v of an incident ion is higher than the thermal velocities of free electrons, the Coulomb logarithm L_{fe} corresponding to the stopping on free plasma electrons is described, according to Ref. [52], in the same way as the Coulomb logarithm in Eqn (4), by substituting the plasma frequency $\omega_p = (4\pi n_{fe}e^2/m_e)^{1/2}$ for the mean frequency $\bar{\omega}$ of atomic electrons:

$$L_{fe} = \ln \frac{2m_e v^2}{\hbar \omega_p} , \qquad (7)$$

where n_{fe} is the bulk density of free plasma electrons. The Chandrasekhar function $G(v/v_e)$ describes a change in Coulomb losses of an incident ion related to averaging its velocity with respect to the thermal velocities of the target's free electrons having Maxwellian distribution. The value of function G tends to unity when the velocity v of the incoming ion is significantly higher than thermal velocities v_e of free electrons. Conversely, if $v \ll v_e$, then $G \to 0$ as $(v/v_e)^3$. Note that formulas (4) and (6) are applicable at incoming particle energies of up to several gigaelectron-volts per nucleon, provided the kinetic energy and the ion velocity are taken in the relativistic limit; contributions S_{fi} and S_{nu} may be neglected for relativistic energies. Moreover, the contribution of ions and nuclei to the plasma stopping power may be disregarded virtually at any velocities of incoming ions. Expressions for S_{fi} and S_{nu} are identical to formula (5), but electron mass m_e in formula (7) must be replaced by ion (nucleus) mass; this done, $S_{fi}(S_{nu}) \ll S_{fe}$ even at an ion energy of ~ 100 keV per nucleon.

This means that theoretically plasma (ionized gas) must possess a higher stopping power than a nonionized gas at an equal density by virtue of two physical causes: (1) a higher effective charge to which fast ions are 'stripped' in the stopping medium, and (2) a larger Coulomb logarithm for free electrons as compared with bound electrons of the cold gas.

The first effect is related to a shift in equilibrium between ionization and recombination processes in plasma toward suppression of the latter due to smaller capture cross sections for free electrons compared with bound ones [49–51]. This effect is most essential for heavy ions with large Z because the ion's effective charge quadratically enters the expression for stopping power [see formula (6)].

The second effect is equally easy to explain because the mean frequency $\bar{\omega}$ of bound electrons in stopping medium atoms is much higher than the frequency ω_p of plasma free electrons.

Thus, the Coulomb logarithm L_{fe} for plasma must be larger than L_{be} for a cold gas of the same density [see formula (7)].

5.2 Experimental investigations into ion stopping processes in a plasma

Theoretical studies on the mechanisms of energy losses by ions in ionized matter have stimulated experimental research in this field at many institutions in this country (ITEP, the All-Russia Research Institute of Experimental Physics, the RAS Institute of Chemical Physics Problems, Chernogolovka) and abroad (GSI, the University of Erlangen, Germany; Institut de Physique Nucléaire, Orsay, France; Sandia National Laboratories, Lawrence Berkeley National Laboratory, USA; Tokyo Institute of Technology, Japan).

Processes associated with ion stopping in an ionized medium are extensively studied with the employment of plasma targets created by external energy sources, viz. discharge in a gas, capillary discharge, laser plasma, plasma of explosive generators, etc., incorporated in the beam transport line emerging from the accelerator (Fig. 11). In this case, a correlation between ion energy losses and the parameters of an ionized substance, viz. the density, temperature and the degree of ionization of the plasma target, turns into the most important aspect for the experiments of a given class.

The first systematic measurements of ion stopping losses in a highly ionized plasma were conducted at UNILAC (GSI) [53] for different types of ions, from ^{40}Ca to ^{238}U, with an energy of 1.4 MeV per nucleon. The target used to measure energy losses of penetrating ion beams was the plasma of a high-current discharge in hydrogen.

The time-of-flight technique was employed in measuring ion energy losses. The authors of Ref. [53] were the first to make use of the high-frequency structure of an ion beam as a reference signal to measure particle energy losses by this method. Ions were recorded with a time resolution of ~ 1 ns by a microchannel plate-based stop-detector. The time dependences of energy losses by uranium, krypton, and calcium ions, as well as plasma density and temperature variations, were detected from the Stark broadening of the H_β-line and by the laser absorption method. Figure 12 compares stopping losses of Pb ions in hydrogen plasma and in cold gas under changes of target linear densities.

Thereafter, a large series of experiments measuring the plasma stopping power for initial ion energies in a range from 1.5 to 11 MeV per nucleon were carried out at GSI [54–57]. These studies showed that ion energy losses in plasma were 1.2–3 times those in cold matter, depending on the initial energy, the particles' atomic charge, and the degree of medium ionization. This result can be accounted for by a higher ion effective charge in the plasma and a larger Coulomb logarithm, in conformity with the theoretical predictions made in Section 5.1.

A sharp rise in the effective charge in the plasma compared with the cold gas (hydrogen) was experimentally
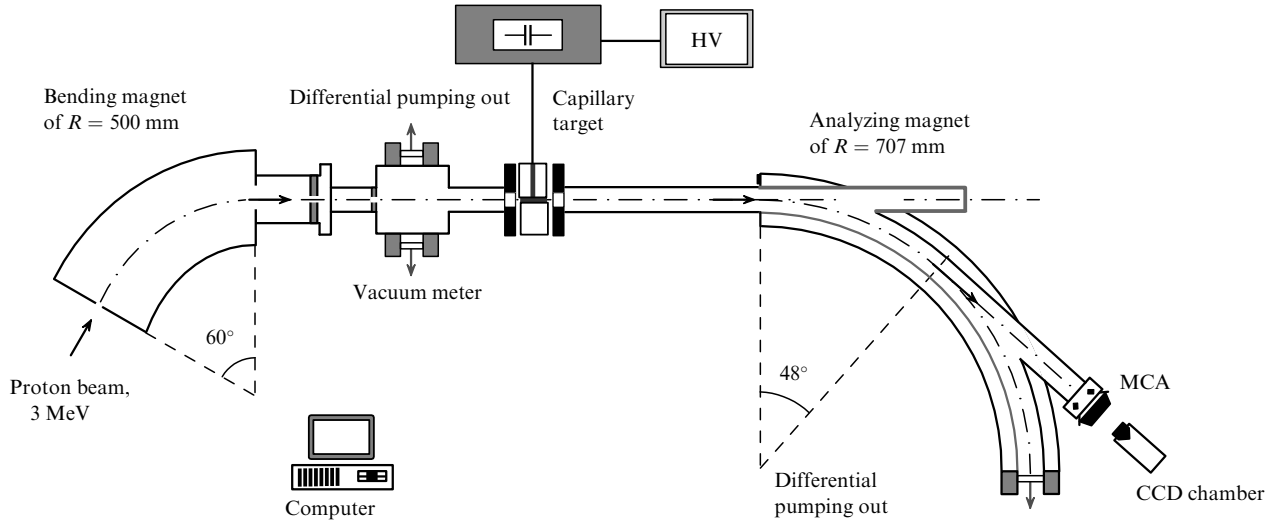
Figure 11. Layout of experiment to measure stopping losses of protons in a plasma target [63]: HV — high-voltage source, and MCA — microchannel analyzer.
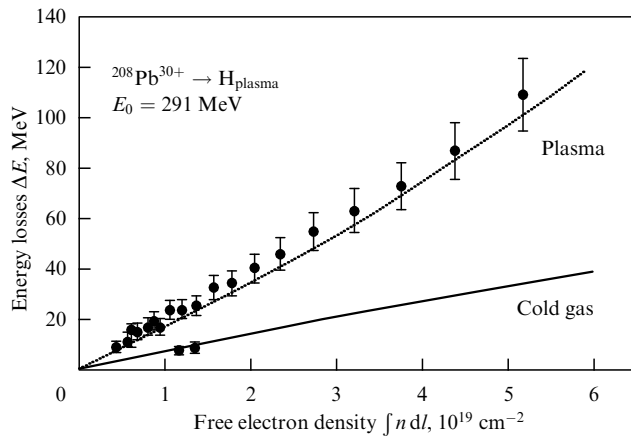

Figure 12. Plots of ion stopping losses versus linear density of the stopping medium [53].

demonstrated in Refs. [56] by magnetospectrometric analysis of the charge composition of ^{40}Ar and ^{129}Xe ion beams with an energy of 5.9 MeV per nucleon, being decelerated in a Z-pinch plasma with a free electron density of $\sim 1.5 \times 10^{19}$ cm^{-3}. At the instant of time when a high-current discharge was propagating through the gas, the charge spectrum of xenon particles showed a marked shift toward the high charge region, from the average charge of $+37$ to $+42$ for ^{129}Xe ions. These data on the effective charge of the ions were compared with the results calculated by the semiempirical Betz formula [58]. This formula, derived from the analysis of experimental data on equilibrium ion charges in gas targets, describes the relationship between the average charge of an ion in the stopping medium and its nuclear charge, depending on the ion velocity normalized to the orbital velocity of electrons.

Of special interest is the range of relatively low ion energies (40–400 keV per nucleon), for which theory predicts the maximum difference between the stopping power of plasma and cold matter in circumstances where Coulomb interactions occur. This maximum arises from the fact that the ion velocity in the beam becomes comparable to the thermal velocity of free electrons in the stopping plasma

medium. Pioneering experiments in this ion energy region were conducted on the high-current heavy ion Maxilac linac at GSI to evaluate stopping losses of ^{84}Kr$^+$ ions with an initial energy of 45 keV per nucleon in ionized matter [59, 60].

The plasma target was a discharge in hydrogen filling a quartz tube 20 cm in length. The 10–20-kA discharge current ensured complete ionization of the hydrogen. Electron density of the plasma measured from the Stark broadening of the H$_\beta$-line amounted to 7×10^{16} cm^{-3} three and a half microseconds after triggering the discharge and gradually decreased to 1×10^{16} cm^{-3} during the next 10 μs. The temperature deduced from the ratio of H$_\alpha$ to H$_\beta$ line intensities and from the ratio of H$_\beta$-line intensity to continuum was 3 eV 4 μs after the onset of the discharge, and fell to 1 eV during the next 10 μs, with the degree of ionization being maintained at the level of $\sim 99\%$. Comparison of stopping losses of ^{84}Kr$^+$ ions in plasma and cold gas revealed a substantial (30-fold and higher!) rise in the stopping power of the totally ionized plasma: 1080 ± 210 MeV mg cm^{-2} and 33 ± 5 MeV mg cm^{-2}, respectively.

A successful experiment on separating the effect of elevated stopping losses of ions in an ionized medium, depending on the growing Coulomb logarithm alone, was conducted jointly by researchers of ITEP and the Institute of Nuclear Physics, Almaty, with the participation of physicists from Germany and France [61].

The experiment measured stopping losses of protons with an energy of 1 MeV in hydrogen plasma. The plasma was generated by an electric discharge in two equally long (78 mm) collinear quartz tubes with oppositely directed currents in the discharge channels. Such an experimental setup permitted weakening the overall focusing effect produced by the magnetic field of the discharge current, because the focusing effects in both channels mutually compensated each other. The initial hydrogen pressure varied from 200 to 900 Pa; as a result, electron number density in the plasma was higher than 10^{17} cm^{-3}.

The diagnostic line of the UKP-1 accelerator (Institute of Nuclear Physics, Almaty), based on an analyzing magnet and electrostatic deflector with the controlled potential difference between the plates, ensured high energy resolution ($\Delta E/E \approx 0.02\%$ for protons with $E = 1$ MeV).

In addition, the authors of Ref. [61] proposed a two-wavelength interferometric technique to study the evolution not only of linear electron density but also of the average degree of ionization in the hydrogen plasma.

The results of independent measurements of the average degree of hydrogen plasma ionization and electron density, taken together with data on energy losses, made it possible for the first time to experimentally evaluate the Coulomb logarithm L_{fe} for the stopping power of plasma free electrons: $L_{\text{fe}} = 14.9 \pm 2.8$ for protons with an energy of 1 MeV. This value coincides, within the limits of experimental error, with the result computed by formula (7) [52], and it is higher than the corresponding value for cold hydrogen: $L_{\text{fe}}/L_{\text{be}} \approx 3$. Because protons at a given energy have an effective charge $Z = +1$ regardless of the degree of ionization and density variations in the stopping medium, the difference observed between stopping losses in the plasma and the cold gas in this experiment was totally due to the distinction between the Coulomb logarithms for free and bound electrons.

In the presence of multiply charged ions, free electrons of the medium affected both the effective charge of the ions and the Coulomb logarithm in the plasma. However, it proved difficult to elucidate how either of these quantities altered in the plasma compared with the cold substance, because the final result always depended on their joint response. A comparative study of energy losses of protons and heavy ions having similar velocities but different masses was carried out to resolve this problem. Simultaneously, charge distribution in ion beams was measured at the plasma target outlet. The study was focused on the plasma produced by a capillary discharge with an evaporating wall (CDEW) in the energy range of incident particles from 3 to 6 MeV per nucleon [62–64].

CDEW plasma reached maximum luminance temperature (3.3 eV) on the third microsecond of the discharge, when the density of free electrons was $(2-6) \times 10^{19}$ cm^{-3}. The authors of Ref. [65] proposed and implemented a new scheme for time-resolved pressure measurements in the plasma using a Michelson interferometer. The maximum pressure in capillaries with diameters of 1.5, 2, and 3 mm was 550, 380, and 240 atm, respectively. Plasma parameters were found to be uniformly distributed along the discharge axis. Stopping losses of protons with an energy of $3-6$ MeV were measured in the CDEW plasma by the time-of-flight technique and a magnetic analyzer with time resolution up to 50 ns. The results were used to compare stopping losses of protons in CDEW plasma and cold polyethylene of equal linear density. Calculations were made using the SRIM code program packet (the Stopping and Range of Ions in Matter) [66] designed to compute energy losses and real ion ranges in a substance based on the quantum-mechanical description of interactions between the test particle and the target's atoms, taking into account Coulomb shielding, excitation and exchange of shell electrons, and the dependence of the effective charge on ion velocity in the medium.

Stopping losses and charge distributions for C, Kr, Pb, and U ions in an energy range of $3.6-11.5$ MeV per nucleon were studied using UNILAC at GSI [63, 64]. Changes in charge distributions in the ion beam behind the capillary target were measured with a dipole magnet having a maximum field of $B = 2.1$ T, while charge-resolved components of the ion beam were detected by a fast plastic scintillator.
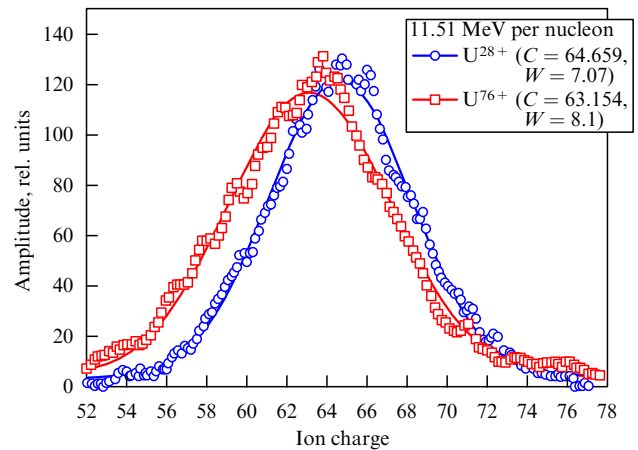

Figure 13. Charge distributions of U^{28+} and U^{76+} ions with an energy of 11.5 MeV per nucleon, measured at the CDEW plasma target outlet [64]; C — average charge, and W — Gaussian distribution parameter.

Energy losses of heavy ions in CDEW plasma were substantially higher (by $20-70\%$, depending on the energy) than the expected theoretical values for an equivalent cold gas, which were obtained with the SRIM code [66]. The difference was due to the increased stopping power of the ionized medium as a result of interactions between ions and free electrons.

Furthermore, an important result was obtained in Refs [63, 64]. The authors observed the dependence of stopping losses on the initial charge of the ions. They experimented with uranium ions having different charges, U^{28+} and U^{76+}, but equal energy, 11.5 MeV per nucleon. Measurements of energy losses and charge distributions of ion beams at the target outlet (Fig. 13) showed that $^{238}U^{76+}$ ions escaping the plasma volume possess a smaller charge and have experienced larger energy losses than $^{238}U^{28+}$ ions with the initially smaller charge.

This effect was attributed to the dependence of the energy loss of an ion on the evolution of its charge during stopping; such a dependence reflects the dynamic balance between ionization and recombination processes, which in turn is a consequence of a decrease in energy in the course of ion stopping [63, 64].

An almost three-fold rise in the stopping power of the fully ionized hydrogen plasma of a gas discharge, compared with that of molecular hydrogen, was demonstrated for bromine and sulfur ions (Br^{6+}, S^{7+}) in an energy range of $0.9-2$ MeV per nucleon in experiments using the electrostatic recharging accelerator in Orsay, France [67, 68]. Moreover, measured variations in charge distributions and stopping losses of chlorine ions in cold hydrogen and totally ionized plasma were compared in Refs [69–71]. The plasma target constituted a linear discharge in hydrogen confined between two fast valves. Such an experimental setup allowed for the first time avoiding the effect of solid foil windows on the energy losses and ion charge distributions being measured. Stark broadening of H_α- and H_β-lines was recorded at each shot. Plasma parameters determined by spectroscopic analysis coincided with the results of plasma density diagnostics by the laser absorption technique and laser interferometry; this gives reason to regard the findings as correct. The ion energy in a beam that passed through the plasma target was determined with a dipole magnet. The effect of the plasma
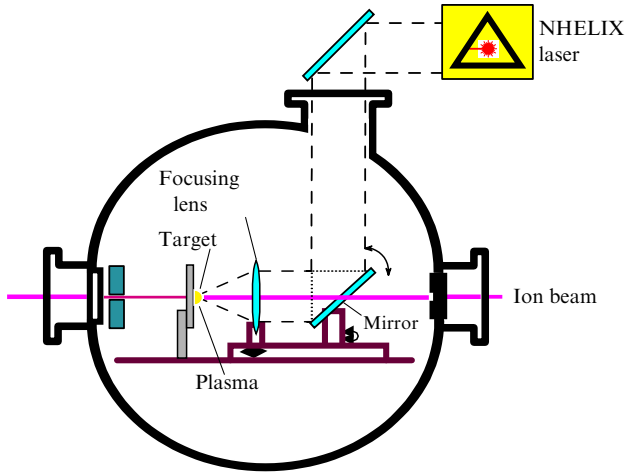
Figure 14. Layout of the experiment for measuring the ion stopping losses in laser-produced plasma [72].

lens was neutralized by a special 'pole-split' magnet that served as a magnetic spectrometer with strong overfocusing. Due to this, the energy for each charge value of chlorine ions was measured to an accuracy of $\Delta E/E = 10^{-4}$. Stopping losses of chlorine ions with an energy of $1.5-2$ MeV a.m.u.$^{-1}$ were measured both in cold hydrogen and in plasma with a similar linear electron density $n_{e}l = 1 \times 10^{19}$ cm^{-2}, where l is the linear plasma size. Furthermore, the experimental evidence for increasing the effective charge of heavy ions in the plasma as against the cold gas was brought forward. This effect was practically indiscernible for chlorine ions with an energy of 2 MeV per nucleon, whereas at 1.5 MeV per nucleon, the average charge at the target outlet for complete hydrogen ionization was higher by unity.

As mentioned earlier, the main ICF issues are related to the region of higher plasma densities and temperatures than in the above experiments. The need for greater plasma densities necessitated installation in UNILAC of a unit for the assessment of stopping losses of heavy ions in the plasma generated by the high-power (100 J for 15 ns) NHELIX (*N*anosecond *H*igh *E*nergy *L*aser for *I*on E*x*periments) neodymium laser (Fig. 14) [72].

The target was made of a $500-2000$ nm thick carbon foil, and the plasma was produced by laser radiation incident on the foil with a power density of $5 \times 10^{9} - 1 \times 10^{11}$ W cm^{-2}. The plasma was formed along a 3 mm length in the direction of beam propagation. Time-resolved spectroscopic measurements in the visible range identified C II and C III lines corresponding to an electron temperature of several electron-volts within 50 ns after the onset of exposure to the laser pulse. Free electron density assessed from the Stark broadening of the spectral lines was 2×10^{20} cm^{-3}. Computer simulation of the laser-produced plasma showed that the initial plasma density of about 10^{21} cm^{-3} fell to 10^{19} cm^{-3} in a time of 100 ns as a result of hydrodynamic expansion. The highest attainable temperature at a flux density of 1×10^{11} W cm^{-2} was 60 eV.

Experiments have recently been made to measure energy losses for various types of heavy ions with energies of 5 and 5.9 MeV a.m.u.$^{-1}$ in foils of different thickness. The measurements were performed by the time-of-flight technique with a base length of 9.4 m. It was shown that stopping losses of ions in the plasma were $2-3$ times those in cold

carbon, depending on the degree of plasma ionization. Based on the charge distribution of ions after their interaction with the plasma, the measured average charge of heavy ions was inferred to be $15-20\%$ higher than the values computed by the Betz formula for gas targets.

Various peculiarities of interactions of protons and ^{16}O ions with plasma produced by irradiation of carbon targets and lithium hydride granules with a high-power neodymium laser were studied in a series of experiments on the electrostatic recharging accelerator at the Tokyo Institute of Technology [73–75]. Laser radiation totally evaporated the lithium hydride granules ($d \approx 60$ μm). Experimentally determined energy losses of oxygen ions in the lithium hydride plasma were $3-6$ times those in cold matter, depending on the incoming particle energy which ranged from 150 to 350 keV per nucleon. Based on the analysis of experimental evidence, the Coulomb logarithm for interactions of protons with an energy of 350 keV per nucleon in plasma turned out to be ~ 1.8 times that in cold matter.

Thus, analysis of the published experimental and theoretical studies of the stopping power of neutral gases versus totally or partly ionized plasma yields the following conclusions:

(1) In a plasma with particle number density below 10^{22} cm^{-3} typical of a gas discharge ($n < 5 \times 10^{19}$ cm^{-3}), the plasma frequency ω_{p} is much lower than the atomic frequency $\bar{\omega}$; in other words, free plasma electrons interact with an incoming particle at higher values of the impact parameter or at lower transferred momenta (which is the same). Therefore, in compliance with Eqn (4) and the above experimental data, ionization of gas leads to enhancing its stopping power by virtue of a larger Coulomb logarithm ($L_{fe} > L_{be}$).

(2) Dynamic processes of ionization and electron capture by an incoming ion in cold and ionized matter are different because the free electron-capture cross section is usually much smaller than that of bound electrons. This accounts for a higher effective charge Z_{eff} of the incoming ion in a totally ionized gas, which is responsible for increased energy losses, also predicted by the theory [46, 47, 49, 50].

5.3 Stopping of particles in a plasma
with strong Coulomb interparticle interactions

The interaction of ions with nonideal plasma (or plasma with strong Coulomb interaction between particles [1, 2]) deserves special consideration. The interparticle interaction parameter (nonideality) is usually represented as $\Gamma = e^{2}(4\pi n_{e}^{1/3}/3)/(k_{B}T_{e})$, where T_{e} is the plasma electron temperature, and k_{B} is the Boltzmann constant. A new approach to the description of the stopping power of a nonideal plasma was proposed, being based on the computation of the effect of an electric field resulting from ion-induced polarization of the medium on the incident ion. Such a 'dielectric' approach to the computation of plasma stopping power yields data substantially (up to ten times) different from those obtained with the extended Bohr–Bethe–Bloch model for ion velocities $v \sim v_{t}$, where $v_{t} = \sqrt{kT_{e}/m_{e}}$ is the thermal velocity of plasma electrons. The results of calculations for high velocities of the incoming ion, $v \gg 10v_{t}$, do not differ. However, the small body of theoretical studies and the lack of experimental data on ion interactions with nonideal plasma ($\Gamma \geqslant 1$) do not provide for applying certain exact formulas to calculating its stopping power.

Basic interest in research on the stopping of charged heavy particles in dense nonideal plasma has arisen in connection
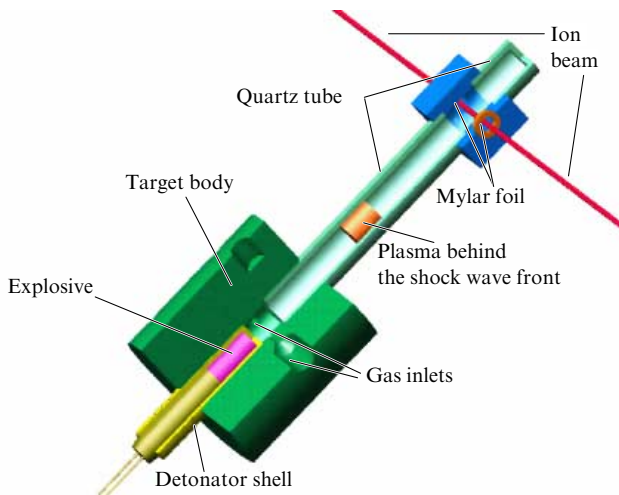
Figure 15. Schematic representation of an explosive generator-based target [88].

Figure 16. Energy losses of 3 MeV protons in a xenon plasma [79] in an explosive generator: *1* — measurements with an analyzing magnet, *2* — measurements by the time-of-flight technique, *3* — total losses in the plasma, *3′* — losses inflicted by bound electrons, *3″* — losses inflicted by free electrons, and *4* — losses in cold gas. Target length equals 6 mm.

with the predicted changes in the quadratic dependence of ion specific energy losses on the effective charge upon reaching the value of $\Gamma \geqslant 1$ as a result of strong Coulomb interactions of stopping medium particles: $\mathrm{d}E/\mathrm{d}x \sim (Z_{\mathrm{eff}})^{\alpha}$ ($\alpha \approx 1.4-1.5$) [76, 77].

Investigations into the effects of strong interparticle interactions at higher plasma densities necessitated the use of an explosive plasma generator [78]. Such generators produce plasma with electron number density $\sim 10^{22}$ cm^{-3}, temperature $1-10$ eV, and nonideality parameter $\Gamma \geqslant 1$ behind the front of a shock wave excited by charge detonation of a chemical explosive in a gas. An important advantage of these plasma generators for beam experiments is the absence of strong electromagnetic fields created when the plasma is produced by a high-current discharge in a gas or a capillary discharge with an evaporating wall.

In experiment [78], the shock wave was excited by blasting a hexagen-type explosive with a mass up to 60 g in a glass or metal tube containing the inert gas Xe (Fig. 15). The tube was placed in a special explosive chamber through which a proton beam from the ITEP Istra-36 accelerator passed. The vacuum explosive chamber 0.88 m in diameter with 25 mm thick walls made it possible to conduct experiments with explosives having a mass below 200 g in a trinitrotoluene (TNT) equivalent.

A beam of protons [79] or ions [80, 81] propagated through the plasma perpendicular to the tube axis. Synchronization of the instant of proton or ion pulse passage through the moving plasma layer with those of the blast and the actuation of the valve system separating the explosive chamber from the vacuum volume of the accelerator was a nontrivial experimental problem. Shock wave velocities (up to ~ 10 km s^{-1}) and the related temperatures, densities, and nonideality parameter $\Gamma \sim 1$ were preliminarily measured. It appears from Fig. 16 that experimental energy losses at large plasma densities were $\sim 30\%$ smaller than those calculated for a plasma of equal linear density.

Systematic studies of stopping losses of C, Ar, Kr, and U ions with different masses and energies from 3.5 to 11.5 MeV per nucleon in xenon and argon plasmas for various types of targets were conducted for the first time based on the UNILAC explosive generator at GSI [81]. Homogeneous plasma structures 4–6 mm in thickness with free electron
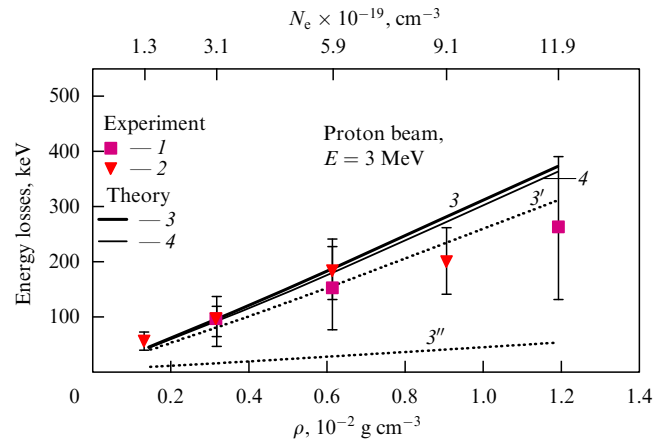
number densities $(0.26-1.5) \times 10^{20}$ cm^{-3} and nonideality parameter Γ ranging $0.6-1.3$ were produced at an initial argon pressure from 0.2 to 3 bar. The dependences of carbon ion energy losses on ionized gas density were also found. Maximum energy losses equal to 2.52 MeV per nucleon were obtained for ions with an energy of 11.5 MeV per nucleon in argon plasma with a linear density of 15.5 mg cm^{-2}.

The 10–20% difference in these experimental results from the ones predicted for ideal plasma (SRIM computations, Ref. [66]) is direct proof of the influence of strong interparticle interaction in an ionized medium on the energy losses of ions in nonideal plasma.

Further experiments with the plasma produced by the explosive generator have the objective of improving the precision of measurements and revealing 'pure' effects of free electrons on ion stopping losses through the use of totally ionized nuclei for test particles.

6. Heating and hydrodynamic motion of matter under the effect of high-power heavy ion fluxes

After specific energy deposition above 100 J g^{-1} ($\sim 10^9$ particles per pulse) was reached using SIS-18 accelerator, experimental studies of the hydrodynamic motion of various substances heated by an ion beam were initiated [82]. The crystals of frozen inert gases Kr and Xe were selected for targets, because they have the lowest sublimation energy.

Framewise shooting of the process with side illumination by a xenon flashbulb (Fig. 17) permitted measurement to be taken of the front velocity (~ 200 m s^{-1}) of lead expanding into the vacuum from a 1 mm thick flat plate irradiated by an ion beam [83].

By diminishing the ion beam focal spot at the target, the researchers managed to reach the level of energy deposition exceeding 1 kJ g^{-1}, and the heated substance extension velocity amounting to 570 m s^{-1} [83]. These data permitted them to estimate substance pressure (~ 2.8 GPa) and temperature (~ 0.17 eV).

Recent progress in enhancing the phase luminance of ion beams by electron 'cooling' and their compression in the longitudinal phase volume [16, 18] allowed a beam of
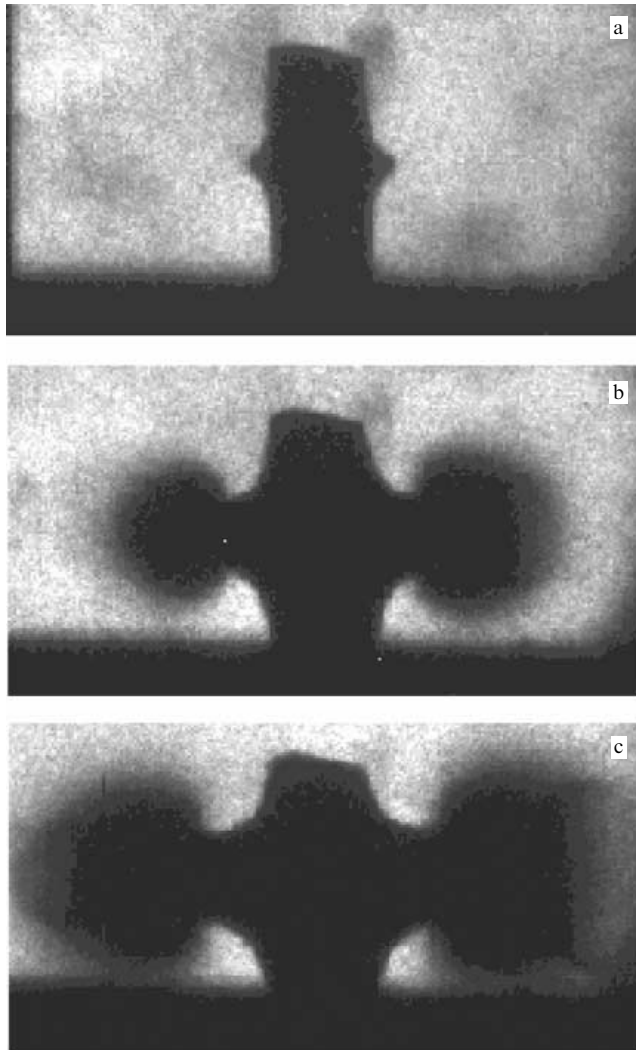
Figure 17. Framewise shooting of the motion of a heated 1 mm thick Pb specimen under the effect of an argon beam with an energy of 300 MeV per nucleon and duration of 300 ns focused on a spot 400 µm in diameter: (a) 360 ns, (b) 1560 ns, and (c) 2360 ns after pulse initiation [83].

$^{238}U^{73+}$ ions with an energy of 350 MeV per nucleon and intensity of $3-4 \times 10^9$ per pulse to be focused on a spot with a diameter $D \leqslant 300$ µm at a pulse length of ~ 110 ns. This made possible measurements of the thermophysical properties and hydrodynamic response of targets from different metals (Pb, W, Ta, Al) and UO_2 to the exposure to an intense ion beam. The temperatures obtained (5000 – 15,000 K) reached the two-phase liquid – gas region and thus permitted studying equations of state and critical points of various materials in the high energy density regime [25].

In connection with these efforts, an international collaboration involving Russian physicists is actively developing special diagnostic tools for dense plasma in the framework of the HIHEX (*Heavy Ion Heating and Expansion*) experiment, making use of SIS-18 ion beams [18]. In this experiment, specimens of solid or porous materials are placed between two transparent sapphire planes (Fig. 18) that restrict expansion of the uniformly heated substance; in this way, a one-dimensional quasi-isentropic regime of hydrodynamic motion toward the gas medium or the vacuum is realized.

Specific experimental conditions characterized by high density and relatively low (~ 1 eV) temperature of the
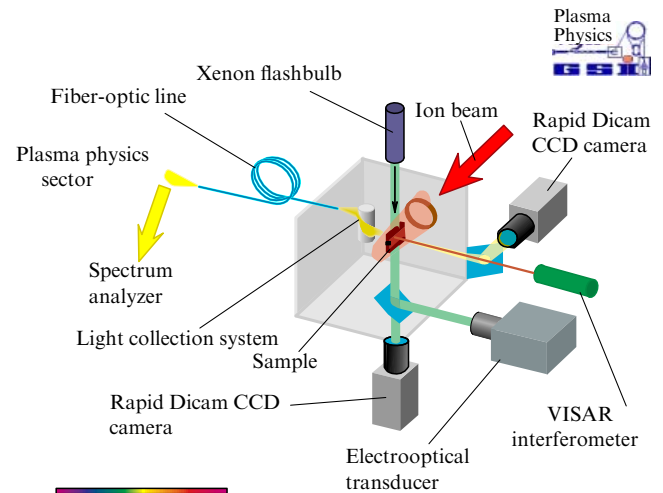

Figure 18. Schematic of the HIHEX experiment [18].

substance impose special requirements on the diagnostics of thermodynamic parameters. Both diagnostic tools developed in the course of research on fast processes in laser plasma and methods used in shock wave experiments with chemical explosives are applicable after relevant modification [1, 2]. An advantage of generating extreme states of matter by ion beams is the rather large volumes of substances studied (a few cubic millimeters) and relatively long characteristic times of variations of thermodynamic parameters ($\sim 10-100$ ns), during which measurements are practicable.

In what follows, the diagnostic techniques of particular importance for heavy ion experiments are reviewed.

Exact ($\pm 5\%$) measurement of the ion beam energy ΔQ absorbed by a study substance is a primary objective in arranging heavy ion experiments. Indeed, this quantity determines one of the main thermodynamic parameters of interest in such investigations, i.e., the specific internal energy of the substance: $\varepsilon_s = \Delta Q$ [kJ g^{-1}]. Evidently, ΔQ depends on the number (N_i) of particles in the beam, the energy release profile along the path of the particles in the target material, and the transverse distribution of ion beam intensity over the focal spot.

The total number of ions in a beam from the accelerator is deduced from current signals coming from the calibrated Rogowski loop placed directly in front of the interaction chamber. The upper limit for the focal spot size is found by recording line emission of argon atoms excited by beam ions in the residual gas [18]. The initial target volume V_0 and density ρ_0 are also specified to a high accuracy.

It was proposed to use γ-radiation induced by inelastic collisions between ions and target nuclei [84]. The intensity of such secondary γ-quanta is directly proportional to the product of ion beam intensity and concentration of target nuclei:

$$\frac{dN_\gamma}{dt} = I_b n_t \sigma(E_i)\Delta l, \tag{8}$$

where Δl is the sample length, and $\sigma(E_i)$ is the cross section of γ-quanta generation.

The main advantages of this method include: (1) the independence of γ-quanta yield from the thermodynamic state of the substance, and (2) the exit of hard γ-quanta from the specimen practically without losses (the target is 'transparent' to γ-quanta with an energy above 1 MeV).
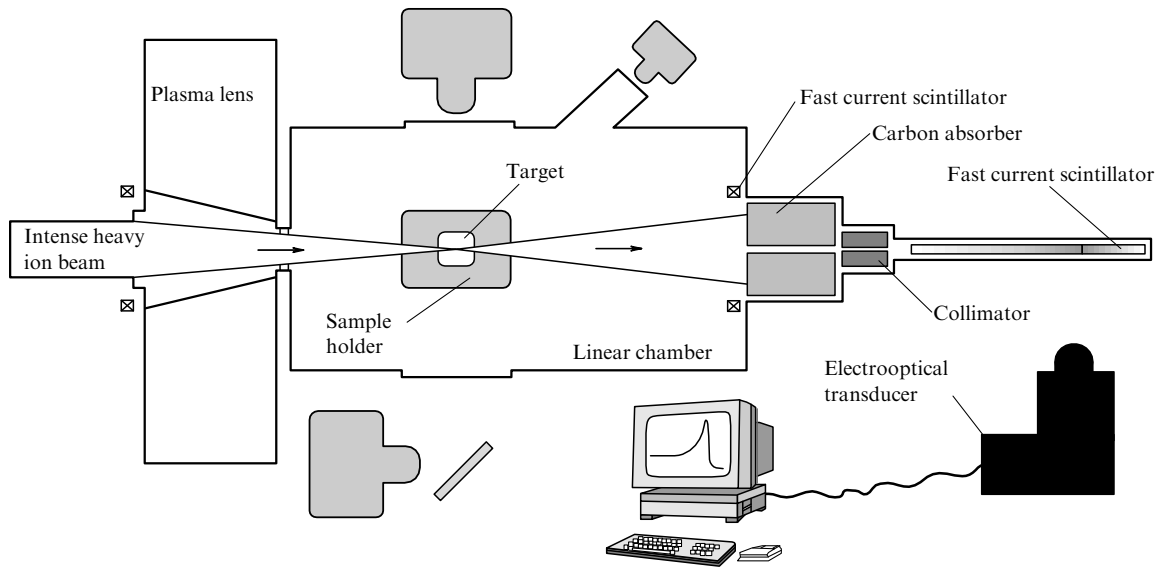
Figure 19. Dynamic spectrometry of energy losses in HED matter [88].

The temperature of dense materials heated to 1000 – 50,000 K by an ion beam is measured by optical pyrometry [85]. Planck spectra are effectively reconstructed using multichannel devices equipped with photodetectors placed behind the narrow-band filters of different thickness in each channel. Such systems possess sufficiently high spatial (~ 100 μm) and temporal (~ 5 ns) resolution and wide dynamic range ($\sim 10,000$). Gauge experiments with tungsten targets [86] yielded time – temperature profiles of specimens heated to a maximum of ~ 6000 K by an ion beam.

The densities of plasma objects are evaluated from measured energy losses of high-energy test particles in the target studied. In the case of protons, it is essential that energy losses depend only on the density of electrons in the stopping medium if their velocities are much higher than the thermal velocity of plasma electrons. The authors of Refs [62, 87] used a beam of protons with an energy of 3 MeV as the test particles to measure the plasma density of a capillary charge at a level of 6.4×10^{19} cm^{-3} at a temperature of 3.3 eV.

Important information on the density of heated matter and other thermodynamic parameters was provided by dynamic measurements of stopping losses in heating ions themselves, when their ranges exceeded the linear size of the target (the so-called dynamic spectrometry of energy losses). It was shown in paper [88] that intense beams of ^{238}U, ^{86}Kr, ^{40}Ar, and ^{18}O ions with an energy of ~ 300 MeV per nucleon interact with cryogenic targets of frozen Ne or Xe gases, heat them, and set their materials in hydrodynamic motion. Particles of the beam that penetrate through the target enter the fast liquid organic scintillator BC-517H and cause luminescence along their path, till they come to a complete stop. The brightest luminescence is observed in the Bragg peak region; thus, the real ion range is determined with high spatial and temporal resolution (Fig. 19).

Because hydrodynamic expansion of the target material results in its reduced linear density, hence in lower energy losses in the target, the position of the Bragg peak in the scintillator undergoes dynamic variations. Energy losses thus measured in the targets can be directly compared with the calculated results to verify physical models (in particular, equations of state) incorporated into software packages. An
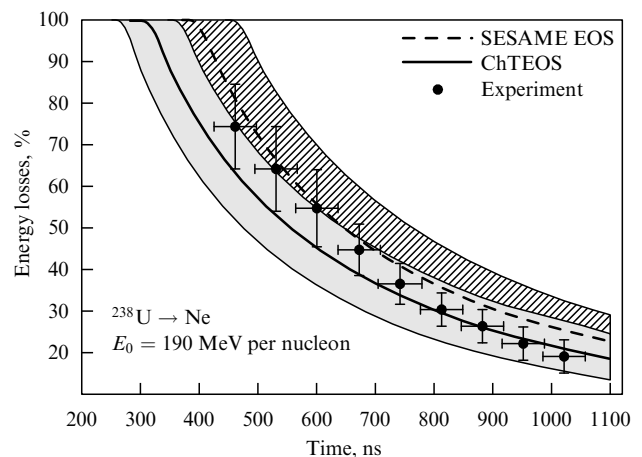

Figure 20. Time dependence of ^{238}U ion energy losses measured during hydrodynamic expansion of the neon target [88] is compared with the dependences calculated by employing different equations of state for the target material: the equation of state (EOS) from the SESAME tables — dashed curve and hatched area, and ChTEOS — solid curve and shaded area.

approximately 1.12 μs ^{40}Ar ion beam ($\sim 5 \times 10^{10}$ ions per pulse) focused by a plasma lens to a spot 0.740 mm in diameter ensured specific energy deposition of ~ 0.57 kJ g^{-1}. Figure 20 compares experimental data on energy losses and theoretical results obtained with regard for the hydrodynamic motion of the target material heated by the intense ion beam. Comparative calculations of particle ranges were made with the use of the SRIM code [66] for cold matter, because target temperature did not exceed 0.5 eV. The hydrodynamic response of the target material (Ne) was evaluated with two-dimensional BIG-2 hydrodynamic code [32] taking into account the real parameters of the heating beam [88] and using SESAME and ChTEOS (Chernogolovka's Temperature Equation of State) equations of state [89].

Comparison of experimental and theoretical data leads to the conclusion that SESAME equations of state in the region of parameters where the correct description of phase transi-

tions is needed are lacking in accuracy, unlike the ChTEOS-based semiempirical model that ensures better agreement.

Dynamic measurements of such parameters of ion-heated matter as volume, the coefficient of volume (linear) expansion, the velocity of boundary motion, and pressure are made by laser shearing interferometers in which the surface of the heated substance is included in one of the arms of the Michelson scheme [90, 91]. The spatial resolution of such systems is restricted to $\sim \lambda/4$, i.e., to ~ 150 nm. Today, new variants of Video Image Stabilization and Registration (VISAR) interferometers are available in which optical fibers and fast photodiodes are employed [92]. The velocities of motion can be measured in a wide range from 10 m s^{-1} to 10 km s^{-1} to a rather high accuracy $(1-2\%)$ with time resolution below 1 ns. Test experiments for the improvement of the method are being carried out with the ion beams of the GSI SIS-18 accelerator in the framework of the international HIHEX experiment [18].

Because plasma transport properties depend on its density and temperature, time-resolved measurements of electrical conductivity provide a wealth of information about extreme states of matter. A method for experiments on measuring the conductivity of plasma heated by heavy ion beams is being developed with the use of a low-inductive electric circuit into which ion-heated specimens are inserted.

The first measurements of conductivity have been made for a number of metals (Pb, Cu, Ag, and Al) [93] at an energy deposition level of 0.5 kJ g^{-1}. Time dependence of lead electrical conductivity that agrees with the conductivity of a normal density metal at a temperature of 0.1 eV was documented.

7. Heavy ion beams in inertial confinement fusion

7.1 High-power drivers-accelerators
In the late 1970s, it was proposed to use an accelerator of intense heavy ion beams as a driver for inertial confinement fusion. The idea stemmed from the possibility of obtaining high-power current pulses based on the known acceleration technologies previously developed for research in high energy physics [15, 94–98].

At present, high-power lasers are under construction in the USA, France, and Russia: the National Ignition Facility (NIF), Laser Mégajoule (LMJ), and Iskra-6, respectively [95, 98, 99]. They are designed to achieve a single act of nuclear ignition of targets containing DT fuel. Nevertheless, ICF with the use of intense heavy ion beams continues to be considered the most promising option in the context of projecting an economically cost-effective nuclear power station. The reason is that heavy ion colliders have a number of well-known advantages, such as

— high efficiency ($\sim 25\%$),

— the confirmed possibility of working at a pulse repetition rate of $\sim 1-10$ Hz,

— high reliability of the driver-accelerator components,

— the possibility of good spatial separation of the final focusing elements and the thermonuclear target itself ($\gtrsim 5$ m).

The required energy levels $(5-100$ GeV) of heavy $(A \sim 200$ a.m.u.) ions and total beam currents (~ 50 kA) do not permit using such heavy ion accelerators as cyclotrons or synchrotrons because of their low efficiency and electric current limitations. Only a linac with an efficiency of $\sim 25\%$ can serve as a driver-accelerator [98]. Two types of such drivers are deemed suitable for the solution of the problem. European designers (including Russian ones) rely on resonant linear accelerators with storage rings [100–102], while their American counterparts tend to use induction linacs [15, 95, 97, 103, 104].

The key issue in the development of any driver-accelerator is the maintenance of ion beam parameters that make it possible to focus a very short (~ 10 ns) and powerful pulse on a small spot far ($\sim 4-5$ m) from the focusing device. This requirement is dictated by the necessity of locating the focusing elements outside a reaction chamber having an inner radius $\geqslant 3$ m. In this case, the achievable size of the focal spot largely determines the total energy (hence, the cost) of the driver ($E_d \sim R_f^{-3}$ [105]) because the ion beam must have a typical power density of order $10^{19}-10^{20}$ W cm^{-2} at a specific energy deposition of ~ 1000 MJ g^{-1} to comply with conditions needed for ignition of the thermonuclear target.

The focusing problem is a crucial one since ions must be physically compressed to a small volume despite Coulomb repulsion forces. The volume charge forces of an ion beam preclude its sharp focusing on the target in the center of the reaction chamber and must be compensated for at least between the last quadrupole lens and the thermonuclear target as the beam is transported toward the latter. Compensation is feasible either by plasma neutralization of the beam (an approach under development in the USA [106, 107]) or by direct charge compensation, as stipulated in the charge-symmetric scheme of the driver-accelerator [101, 108].

Relevant scaling experiments on the transport of intense ion beams through plasma channels are currently underway at LBNL, Berkeley [106] and at GSI [107]. The experiments are timed to coincide with detailed numerical simulation of processes taking place in accelerators, all the way from the ion source through the beam transport channel toward the target inside the reaction chamber, using three-dimensional (3D) computer codes [109, 110].

7.2 Targets for heavy ion inertial fusion
Similar to laser targets, heavy ion ICF targets are categorized into directly and indirectly irradiated ones. In one-dimensional calculations, the former ensure much higher gain coefficients G than the latter (X-ray) targets simply due to the absence of an additional stage of ion beam energy conversion to X-ray radiation. However, the use of directly irradiated targets is associated with negative two- and three-dimensional effects inevitably produced by inhomogeneities of frontal irradiation. For this reason, researchers all the world over have concentrated their efforts on working with indirectly irradiated targets in which fuel implosion occurs via the intermediate stage of ion beam energy conversion to the energy of thermal X-ray radiation with characteristic temperatures $T_X = 100-300$ eV [105, 111–115]. The main feature of indirectly irradiated targets is spatial separation of the absorption region (converter) of irradiating ions and the accelerated spherical sheath of the DT fuel with the adjoining outer layer of the capsule (Fig. 21). Energy transfer from the converter to the DT-capsule is realized only by means of X-ray radiation.

The optimal design of a heavy ion target needs to be substantially modified if heavy ion beams with relatively high (almost relativistic) energies, $E_i \geqslant 0.5$ GeV per nucleon, are chosen as a driver [100, 108].
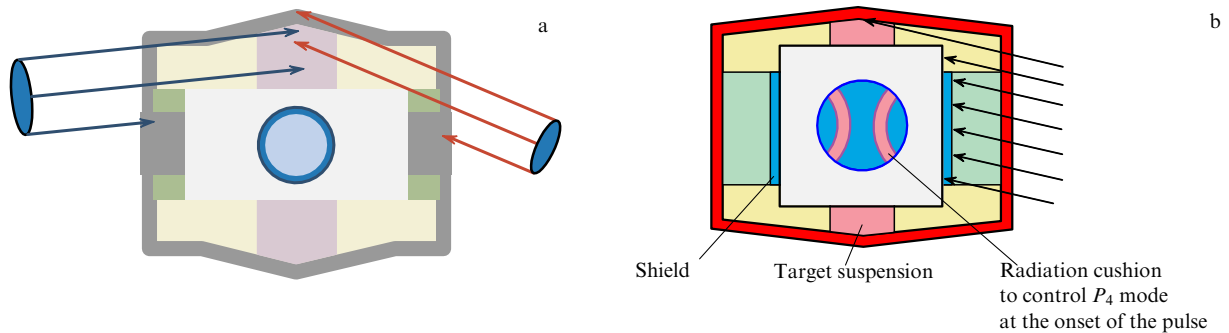
Figure 21. (a) Target with a distributed converter for 120 beams with an angle of incidence up to 24°. (b) Hybrid target with a large-sized focal spot irradiated by ion beams at a small angle of incidence [115].

Heavy ions with energies $E_i \geqslant 0.5$ GeV per nucleon have relatively long ranges ($R \geqslant 5-20$ g cm^{-2}) that are virtually incommensurable with the spherical geometry of fuel compression. The proposed cylindrical target responds to two separate ion pulses traveling along the cylinder axis [100, 115]. One- and two-dimensional calculations reveal that the minimal ion beam energy needed for cold compression of DT fuel in directly irradiated cylindrical targets varies from 10 to 15 MJ cm^{-1}. Ignition and propagation of the combustion wave along the cylinder can be achieved with a second powerful heavy ion beam 0.2 ns in length at a total pulse energy of 0.4 MJ ('fast ignition principle') [116, 117]. Based on the results of two-dimensional calculations, the fuel burnup fraction is $f_b \approx 0.4-0.6$. In this case, the thermonuclear gain of the target amounts to $G = 50-150$ [113].

7.3 Concepts of the reactor chamber and the inertial fusion power plant

The energy characteristics of a nuclear power plant depend first and foremost on the amplification factor of the power-generation cycle K_e. In the case of ICF, it is the product of driver efficiency η, target gain G, heat cycle efficiency ε, and power gain in the reactor blanket M; in fact, it equals the ratio of the electric power of the plant to the power consumed for feeding the driver:

$$K_e = \frac{P_e}{P_d} = MG\eta\varepsilon. \tag{9}$$

As known [95, 98], the cost of electric energy grows rapidly for $K_e < 4$, when the driver consumes over 25% of the produced electric power. Typical values of the parameters entering into formula (9) are as follows: $M = 1-1.2$ and $\varepsilon = 0.3-0.35$. Therefore, the product ηG must be higher than 10. This accounts for the advantages of heavy ion drivers over other types of these machines. Their efficiency $\eta \sim 25\%$ permits setting up a realistic claim for the value of target gain G, i.e., to design targets with $G = 50-100$. Since the cost of a driver grows progressively with its energy, the development of efficient driver facilities and targets with the highest thermonuclear gain G and the lowest possible energy is the principal goal in ICF.

The results of an economic analysis by several research groups indicate that the production cost of electric power produced in ICF is competitive when a 10 Hz driver operates on 5 reactors with a thermal capacity of ~ 1 GW each [95, 98].

The most important advantage of an ICF reaction chamber is the possibility of using the liquid first wall responsible for the long (~ 30 years) reactor lifetime [97, 118]. Indeed, the liquid wall not only takes upon itself the primary impact of microexplosion products (with an energy equivalent to $\sim 100-200$ kg of a chemical explosive) and protects the solid wall from fast neutrons ($\sim 80\%$ of the energy flux), γ-radiation ($\sim 10\%$), plasma and target debris ($\sim 10\%$), but also performs additional functions, namely

— it serves as a coolant transporting heat to the steam-turbine cycle;

— it acts as a 'cryopump': due to the low pressure of saturated vapor ($\sim 10^{-5}$ Torr at $\sim 500\,^\circ$C) it creates, within less than 200 ms after the explosion, a vacuum ($\sim 10^{-3}$ Torr) in the reaction chamber, needed for the next microexplosion to occur;

— it contains lithium and therefore serves as material for tritium production.

Liquid lithium-containing eutectics with an operational temperature of $\geqslant 500\,^\circ$C are usually used as multifunctional coolants.

A number of conceptual projects for ICF-based reactors coupled to a laser driver, heavy ion accelerator [118–121], or powerful pulsed discharge have been proposed. A mutually consistent driver–target–reactor chamber assembly looks especially advantageous when using a heavy ion driver, because it reduces to a minimum the number of windows for the injection of radiation into the chamber, and the magnet focusing lenses are not directly affected by neutrons. A concept presented in Refs [122, 123] describes a reaction chamber and a thermal scheme of an ICF power plant designed for a thermal capacity of 1 GW, driven by heavy ions with an energy of 100 GeV, and having a directly irradiated cylindrical target for fast ignition by the ion beam.

The progress in theoretical and experimental research on heavy-ion-driven ICF continues at an increasing rate in Europe, Russia, and the US. It extends now to the physics of powerful heavy ion accelerators, intense beam–plasma interactions, high energy density in matter, and targets for heavy-ion-driven ICF, along with special problems of heavy ion reactors. Serious efforts have been made over the last years to refurbish the existing ITEP accelerator complex. The upgraded machine will be indeed the world's first high-power heavy ion facility, bringing an appreciable change for the better in the field of interest [17, 124]. The use of the previously available equipment and instrumentation permits substantially reducing the cost of the project without detriment to performance characteristics of the modernized facility (rated beam power ~ 1 TW, and accumulated energy ~ 100 kJ). They are expected to provide an opportunity for

breakthrough experiments on heavy-beam-driven ICF. Such experiments may primarily include intense ion beam acceleration and accumulation physics, interaction of intense ion beams with plasma, and fundamental HED matter physics.

8. Conclusions

This review paper shows how the physical properties of Nature manifested in the processes of stopping intense heavy ion beams in matter make relativistic heavy ion colliders powerful energy sources (drivers) that find application in research on extreme states of matter. Due to the volumetric character of ion energy release, intense heavy ion beams can generate different states of matter, including those with an exotic set of thermodynamic parameters, and provide a unique tool for investigations into extreme states of matter under reproducible experimental conditions.

Experiments with heavy ion beams are currently underway by a wide international collaboration based on the SIS-18 (Darmstadt) and TWAC (ITEP) accelerators. They include studies of equations of state, plasma phase transitions, critical points of metals, conductivity, noncongruent phase transformations, and atomic physics covering strong interparticle interactions.

Heavy ion beam experiments have important practical implications for inertial confinement fusion, nuclear reactor safety, plasma technologies, and planetary geophysics. It has been shown that the heavy ion driver has the most important advantage over other types of similar machines because its efficiency ($\sim 25\%$) permits advancing a realistic claim for the value of target thermonuclear gain G, i.e., to design targets with $G = 50 - 100$. Therefore, the development of efficient drivers-accelerators and targets with the highest coefficient G of thermonuclear amplification and the lowest possible driver energy is the primary goal in ICF.

9. Appendix. Hadron beam therapy

As shown in Section 3, the energy release profile of an ion beam has a characteristic peak in the end of the ion's path. In the late 1960s, it was proposed to use this important property of hadrons (protons and ions) for the *in vivo* precision treatment of malignant neoplasms [125 – 127]. Thus, medical sections were attached to large proton accelerators in Berkeley, USA, and at ITEP, USSR that first carried out radiobiological studies, and thereafter proceeded to actual clinical work. The success of proton therapy starting in the early 1990s provided a basis for setting up specialized centers that annually admit hundreds and thousands of patients. These centers comprise compact proton accelerators with energies up to 300 MeV and beam splitting systems to deliver a beam to 4 or 5 treatment rooms equipped with precision devices for remote directed action on malignant neoplasms (MNs). The possibility of using carbon ions of the SIS-18 accelerator in Darmstadt for medical purposes opened a new page in hadron therapy. Carbon ions have a higher atomic charge than protons; this accounts for their more efficacious action on the affected body area, while minimizing irradiation to the surrounding healthy tissue. Moreover, carbon ions do not induce undesirable biochemical reactions, since this element is a natural constituent of living molecules. The available clinical experience is now being applied to design and construct a specialized center for carbon therapy in Heidelberg, where the carbon ion accelerator will be used to treat brain tumors.

Rapid development of hadron therapy is being promoted by two factors [128]:

First, maximum reduction in radiation exposure of healthy organs and structures by minimizing the treatment field and/or the dose absorbed by the normal tissue. The dose of radiation delivered to a tumor (target) is practically always limited by the allowable exposure rate for healthy tissues, which inevitably suffer when the radiation load on the target increases; such an increase determines the number (frequency) and severity of post-radiation complications.

Proton beams permit reducing the radiation load better than other types of ionizing radiation. Comparison of γ-irradiated and proton-irradiated patterns of the same target indicates that the latter results in an almost two times lower radiation load on normal healthy tissues than the former.

Moreover, proton beams create a very high radiation dose gradient at the posterior and lateral boundaries of the treatment field due to certain peculiarities of their passage through the tissue. This fact opens up two absolutely new possibilities for radiotherapy:

- irradiation of small and ultrasmall targets;
- irradiation of targets located very close to critical (highly radiation-sensitive) organs and structures.

Proton therapy can be used to manage neoplasms in children, as well as tumors of the head, neck, lungs, bones and soft tissues, gastrointestinal tract, nervous and urogenital systems, and gynecological organs.

Second, hadron therapy permits better differentiating between the responses of malignant cells/tumors and normal tissues to the same absorbed radiation dose. This fact is of primary importance in the context of treatment of radioresistant neoplasms and its improvement.

For some radiobiological reasons, dense ionizing radiation (π^--mesons, neutrons, ions heavier than protons) overcomes radioresistance of malignant neoplasms unaided by special modifiers. The efficiency of treatment of radioresistant tumors by neutron beams (neutron and neutron capture therapy) and beams of ions heavier than protons is pretty well confirmed and universally recognized. Among heavy ions, carbon ions appear to be most extensively used for radiotherapy [131, 132] by virtue of their high biological efficiency and ability to overcome radioresistance, compared with lighter ions.

The combination of these two properties, viz. high biological efficiency and the possibility of creating sharply outlined high dose gradients at the boundaries of treatment fields, accounts for the higher efficiency of carbon ion beams in the radiation therapy of radioresistant tumors compared with neutron beams that are unable, in principle, to produce a similar well-outlined dose distribution pattern.

Situation throughout the world
From 1954 till 1990, all clinical studies were carried out in research centers based on physical (not medical) accelerators. The world's first health center for proton therapy in Loma Linda, USA, having a specialized medical accelerator, began regular operation in 1990, after the successful outcome of therapeutic irradiation had been documented. Since then, the number of clinical (not experimental) centers for hadron

Table 2. Progress in building centers for hadron therapy.

Type of center ＼ Year	1988	1990	2005	2006	2015 (expected)
Experimental centers	11	13	20	20	20
Clinical centers	—	1	11	20	35
Total	11	14	31	40	55

therapy has been growing at an ever-increasing rate [129, 130] (Table 2).

Three centers for carbon ion therapy have been operating in the world and construction work is underway for four others to complement the existing therapeutic proton facilities that all are accumulating the results of radiobiological, preclinical, and clinical studies. Construction of ion therapy centers is forging ahead fast, and it is anticipated that there will be almost as many of them in the near future as hospitals for proton therapy.

Proton therapy centers are equipped under a turnkey contract by many well-known companies (Mitsubishi, Hitachi, IBA, Siemens, and others). The cost of a center varies from US $70 to 100 mln, depending on its design and local conditions.

Situation in Russia

Three experimental centers of proton therapy (PT) have been operating in Russia since 1967. These are the PT Center of the Joint Institute for Nuclear Research, Dubna (since 1967, over 500 patients), the PT Center of ITEP, Moscow (since 1969, 4000 patients), and the PT Center of the Central Research Roentgeno-Radiological Institute and B P Konstantinov Petersburg Institute of Nuclear Physics, Gatchina (1974, some 1300 patients). By 1990, when the first clinical PT center was opened in Loma Linda, USA, almost one third of the total world number of patients treated by proton therapy (about 3000) lived in the USSR. Further developments in hadron therapy practically stopped in this country after 1990. Since then, the annual number of patients using the services of the PT centers has been decreasing, in contrast to other countries, where it continues to grow steadily (Fig. 22a). The first specialized regional project based at S P Botkin City Clinical Hospital, Moscow was initiated only in 2006 and now is progressing (Fig. 22b).

The design of the new PT center incorporates the very latest in state-of-the-art hospital facilities. The course of project implementation shows that it can be successfully completed through the efforts of Russian developers and manufacturers themselves.

Clinical requirements for the assembly, structure, and major characteristics of hadron therapy centers (HTCs)

Requirements for the assembly, structure, and major characteristics of clinical centers ensue from the following generally accepted and approved principles:

(1) The center must only be integrated into a large modern hospital having well-equipped oncological and radiological departments, relevant diagnostic (topometric) expertise, and technical means for conventional (X-ray, gamma-particle, electron) radiotherapy.

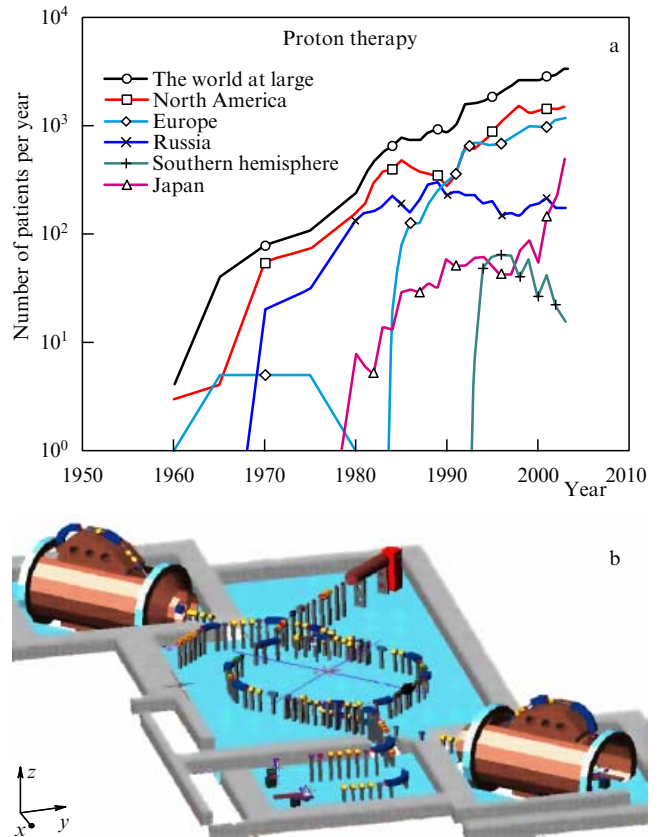If appropriate, such a hospital needs to be established simultaneously with the HTC.

Figure 22. (a) Annual number of patients by countries and continents [131]. (b) Projected PT Center at S P Botkin City Clinical Hospital, Moscow (therapeutic floor) [132]: 250 MeV synchrotron (in the middle); injector (linac) (top right-hand corner); rotational irradiation units to treat patients in the supine position (upper left-hand and bottom right-hand corners); fixed horizontal beam room with two irradiation facilities (in the center). The novelty of the project consists in simultaneous patient irradiation in all three treatment sections.

(2) The HTC must be designed to use either two types of radiation (proton and ion beams) or only one of them.

(3) The major HTC components are the accelerator, hadron beam units, topometric and imaging systems for planning radiotherapy, and competent information support.

(4) The accelerator is an indispensable but not the most important and expensive component of an HTC. Any type may be used, viz. synchrotron, cyclotron, or linac. The main characteristics of the facility are reliability and a long lifetime (continuous operation without repairs or preventive maintenance). Main parameters of the beam must be such as to ensure irradiation of both small and large (a few liters in volume) malignant neoplasms located in any part of the body. Modern acceleration technologies provide beams with the parameters necessary to achieve the required dose distribution patterns at hadron energies of up to 300 MeV per nucleon.

(5) Three to five treatment rooms are needed to perform each procedure (proton therapy, ion therapy), with two to four of them housing proton beam units for rotational and multifield irradiation of patients in a fixed horizontal position using a gantry system. The beam must be fed into one of the rooms for ion therapy in three planes, i.e., horizontally, vertically downward, and at 45° from the top. One or two rooms are equipped with horizontal-beam systems (for oncoophthalmology and radioneurosurgery). There must be

at least three rooms for each treatment modality (proton therapy, ion therapy); the annual flux of patients (1000 or more) depends on economic considerations.[3] The maximum number of treatment rooms (no more than five) is limited by the capacity of a single hadron source (accelerator) to generate beams for more irradiation units. The relative number of gantry-equipped treatment rooms and those fed by horizontal beams is determined by the fact that the latter can be used to treat only certain specifically located malignant neoplasms (5–7% of their total number). At present, operation of an HTC without gantry systems is considered impractical. Gantry allows a patient to be irradiated unrestrictedly from any angle (4π). Introduction of limitations would make proton therapy noncompetitive compared with conventional radiotherapeutic modalities (X-rays, gamma-particles, and electrons).

(6) Effective exploitation and functioning of sophisticated HTC equipment are possible only if supported by modern information technologies, such as the specialized Radiological Information System (RIS). This system comprises high-capacity sources of 3D-topometric information coupled to powerful workstations for pre-irradiation treatment and imaging systems with a superimposed radiotherapy plan. RIS is an important tool for the integration of general clinical information into the system of manipulation of irradiation units for the successful accomplishment of therapeutic protocol.

(7) The availability of conventional radiotherapeutic equipment listed in item 1 is mandatory to guarantee continuation of the treatment of *all* (up to 100) admitted patients in the event of hadron accelerator breakdown. This equipment represents the necessary backup.

(8) The most important clinical requirement is meeting dose distribution specifications. Taken together with beam unit characteristics, they determine the scope of applications of hadron therapy and its clinical utility. Softening these requirements always narrows the sphere of applications and compromises the clinical outcome of hadron therapy.

Summary

Hadron therapy is a natural step in the development of remote radiotherapy.

(1) Hadron therapy improves local control of malignant neoplasms (especially small and very small ones), reduces the incidence and severity of post-irradiation complications, makes possible the treatment of radioresistant neoplasms and those located close to vitally important organs and structures of the body.

(2) Design and construction works for clinical centers of proton and ion therapy are well underway throughout the world. They will treat many oncological patients in the near future.

(3) Thus far, only three experimental centers of proton therapy have been operating in Russia (Moscow, Dubna, Saint-Petersburg). A total of 5800 patients have been treated (roughly 12% of the world total). Most of them (4000) received radiotherapy in the PT Center of ITEP.

(4) Hadron therapy being a most efficacious up-to-date radiotherapeutic modality, Russia needs a central HTC with branches in different regions of the country.

(5) As yet, only one regional project of a PT center is nearing implementation, based at the S P Botkin City Clinical Hospital. The project is financed by the Government of Moscow. It is being realized under the scientific auspices of the Russian Federation State Scientific Center 'A I Alikhanov Institute of Theoretical and Experimental Physics' (general designer).

(6) Experience gained in the work on the Moscow HTC indicates that similar projects for other regions of Russia can be successfully completed through the efforts of domestic developers and manufacturers (research institutions and industrial enterprises) based on the scientific and economic potential of the country.

(7) A special federal program is needed to address the problem. It should envisage the development of a central HTC and its regional branches to meet the demands of domestic and foreign users. The program may be most successfully realized in the framework of the national project Health Care and/or the federal task program Research and Development in the Priority Fields of Science and Technology in Russia for 2007–2012.

(8) Construction of new HTCs will greatly contribute to the further improvement of oncological services in Russia, the quality of which is still greatly inferior to that provided in other developed and even developing countries.

(9) HTCs may be either full-scale (proton and ion) therapeutic facilities or provide only one of these options. The cost of major nonstandard equipment (accelerator, beam transport channels, irradiation units, etc.) in central HTC amounts to 3.65 billion rubles (proton and ion therapy), 2 billion (proton therapy), or 2.2 billion (ion therapy). The cost will vary, depending on the number of beam units. One to two billion rubles worth of standard conventional medical equipment will be needed, depending on its availability in the base hospital.

(10) Design and construction works for a central HTC may be completed within 4–5 years. The commissioning schedule is as follows: design of nonstandard equipment will take 2 years; its manufacture 2 years; building of a hall for installation of the equipment 1.5–2 years, and assembly, testing, and putting into operation 1–1.5 years. Optional equipment may be developed and manufactured totally by domestic enterprises, such as ITEP, the D E Efremov Research Institute of Electrophysical Apparatus, the Institute for High Energy Physics, and the Joint Institute for Nuclear Research.

References

1. Fortov V E, Khrapak A G, Yakubov I T *Fizika Neideal'noi Plazmy* (Nonideal Plasma Physics) (Moscow: Fizmatlit, 2004)

2. Fortov V E *Moshchnye Udarnye Volny i Ekstremal'nye Sostoyaniya Veshchestva* (Powerful Shock Waves and Extreme States of Matter) (Moscow: Bukos, 2005)

3. Davidson R (Ed.) *Frontiers of High Energy Density Physics* (Washington, D.C.: NRC, Natl. Acad. Press, 2003)

4. Atzeni S, Meyer-ter-Vehn J *The Physics of Inertial Fusion* (Oxford: Clarendon Press, 2004)

5. Al'tshuler L V *Usp. Fiz. Nauk* **85** 197 (1965) [*Sov. Phys. Usp.* **8** 52 (1965)]; Al'tshuler L V et al. *Usp. Fiz. Nauk* **169** 323 (1999) [*Phys. Usp.* **42** 261 (1999)]

6. Al'tshuler L V et al. *Vestn. Ross. Akad. Nauk* **74** 1011 (2004) [*Herald Russ. Acad. Sci.* **74** 613 (2004)]

7. Vladimirov A S et al. *Pis'ma Zh. Eksp. Teor. Fiz.* **39** 69 (1984) [*JETP Lett.* **39** 82 (1984)]

---

[3] The cost of an accelerator usually accounts for 20–25% of the total HTC cost. A reduction in the number of treatment rooms increases the cost of the accelerator per room.

8. Trunin R F *Usp. Fiz. Nauk* **164** 1215 (1994) [*Phys. Usp.* **37** 1123 (1994)]
9. Avrorin E N et al. *Usp. Fiz. Nauk* **163** (5) 1 (1993) [*Phys. Usp.* **36** 337 (1993)]
10. Karsch F "Lattice QCD at High Temperature and QGP", BNL-NT-06/2; hep-lat/0601013
11. Ginzburg V L *O Fizike i Astrofizike* (Physics and Astrophysics: a Selection of Key Problems) (Moscow: Nauka, 1985) [Translated into English (Oxford: Pergamon Press, 1985)]
12. Müller B, Nagle J L "Results from the Relativistic Heavy Ion Collider" *Annu. Rev. Nucl. Part. Phys.* **56** 93 (2006)
13. Kolomenskii A A *Fizicheskie Osnovy Metodov Uskoreniya Zaryazhennykh Chastits* (Physical Principles of the Methods for Charged Particle Acceleration) (Moscow: Izd. MGU, 1980)
14. Tahir N A et al. "The CERN Large Hadron Collider as a tool to study high energy density matter" *Phys. Rev. Lett.* **94** 135004 (2005)
15. Bock R et al. "Inertial confinement fusion: heavy ions", in *Landolt-Börnstein*, New Series, Group VIII/3B *Energy Technologies*, Sub-volume B: *Nuclear Energy* (Heidelberg: Springer-Verlag, 2005) p. 529
16. Hoffmann D H H et al. "Frontiers of dense plasma physics with intense ion and laser beams and accelerator technology" *Phys. Scripta* **T123** 1 (2006)
17. Alekseev N N et al. "Fizicheskii zapusk nakopitel'nogo kol'tsa TVN" *At. Energ.* **93** 474 (2002) ["Physical startup of the TWAC storage ring" *At. Energy* **93** 995 (2002)]
18. Hoffmann D H H et al. "Present and future perspectives for high energy density physics with intense heavy ion and laser beams" *Laser Part. Beams* **23** 47 (2005)
19. Henning W F *Nucl. Instrum. Meth. Phys. Res. B* **204** 725 (2003); **214** 211 (2004)
20. Neumayer P et al. "Status of PHELIX laser and first experiments" *Laser Part. Beams* **23** 385 (2005)
21. Alekseev N N, Koshkarev D G, Sharkov B Yu "Neliuvillievskoe nakoplenie yader ugleroda v uskoritel'no-nakopitel'nom komplekse ITEF" *Pis'ma Zh. Eksp. Teor. Fiz.* **77** 149 (2003) ["Non-Liouvillian carbon nucleus accumulation at the ITEP storage accelerator facility" *JETP Lett.* **77** 123 (2003)]
22. Sigmund P *Particle Penetration and Radiation Effects* (Berlin: Springer-Verlag, 2006)
23. Bakhmetjev I E et al. "Research into the advanced experimental methods for precision ion stopping range measurements in matter" *Laser Part. Beams* **21** 1 (2003)
24. Arnold R C, Meyer-ter-Vehn J "Heating matter with heavy ion beams" *Z. Phys. D* **9** 65 (1988)
25. Hoffmann D H H et al. "Unique capabilities of an intense heavy ion beam as a tool for equation-of-state studies" *Phys. Plasmas* **9** 3651 (2002)
26. Zel'dovich Ya B, Raizer Yu P *Fizika Udarnykh Voln i Vysokotem-peraturnykh Gidrodinamicheskikh Yavlenii* (Physics of Shock Waves and High-Temperature Hydrodynamic Phenomena) 2nd ed. (Moscow: Nauka, 1966) [Translated into English (Mineola, NY: Dover Publ., 2002)]
27. Sokolowski-Tinten K et al. "Transient states of matter during short pulse laser ablation" *Phys. Rev. Lett.* **81** 224 (1998)
28. Batani D et al. "Measuring equation of state with lasers" *Europhys. News* **27** 210 (1996); "Equation of state data for iron at pressures beyond 10 Mbar" *Phys. Rev. Lett.* **88** 235502 (2002)
29. Korobenko V N et al. *Fiz. Plazmy* **28** 1093 (2002) [*Plasma Phys. Rep.* **28** 1008 (2002)]; Gathers G R *Rep. Prog. Phys.* **49** 341 (1986)
30. Kozyreva A et al. "Dynamic confinement of targets heated quasi-isochorically with heavy ion beams", GSI-2003-2 Annual Report (2003) p. 27; *Phys. Rev. E* **68** 056406 (2003)
31. Gregori G et al. *Phys. Rev. E* **67** 026412 (2003)
32. Fortov V E et al. *Nucl. Sci. Eng.* **123** 169 (1996)
33. Sharkov B Yu et al. "Heavy ion fusion energy program in Russia" *Nucl. Instrum. Meth. Phys. Res. A* **464** 1 (2001)
34. Basko M M, Churazov M D, Aksenov A G *Laser Part. Beams* **20** 411 (2002)
35. Piriz A R et al. "Generation of a hollow ion beam: calculation of the rotation frequency required to accommodate symmetry constraint" *Phys. Rev. E* **67** 017501 (2003)
36. Basko M M *Phys. Plasmas* **7** 4579 (2000)
37. Kazarin A et al. "Chislennoe modelirovanie tsilindricheskoi kompressii misheni s vnutrennei oblast'yu s maloi plotnost'yu" ("Numerical simulation of cylindrical compression with internal region and low density"), GSI-2001-4 Annual report (2000) p. 48
38. Basko M M, Kemp A J, Meyer-ter-Vehn J *Nucl. Fusion* **40** 59 (2000)
39. Churazov M D, Sharkov B Yu "Heavy-ion targets without tritium" *Nuovo Cimento A* **106** 1945 (1993)
40. Tahir N A et al. *Phys. Rev. E* **63** 016402 (2001)
41. Tahir N A et al. *Contrib. Plasma Phys.* **41** 287 (2001)
42. Tahir N A et al. "Intense heavy ion beams as a tool to induce high-energy-density states in matter" *Contrib. Plasma Phys.* **43** 373 (2003)
43. Ebeling W, Richert W *Contrib. Plasma Phys.* **25** 431 (1985)
44. Devald E, Constantin C *Ann. Rep.* (2001)
45. Tahir N A et al. "The creation of strongly coupled plasmas using an intense heavy ion beam: low-entropy compression of hydrogen and the problem of hydrogen metallization" *J. Phys. A: Math. Gen.* **36** 6129 (2003)
46. Nardi E, Zinamon Z *Phys. Rev. Lett.* **49** 1251 (1982)
47. Peter T, Meyer-ter-Vehn J *Phys. Rev. A* **43** 1998 (1991)
48. Mehlhorn T A *J. Appl. Phys.* **52** 6522 (1981)
49. Basko M M *Fiz. Plazmy* **10** 1195 (1984) [*Sov. J. Plasma Phys.* **10** 689 (1984)]
50. Deutsch C et al. *Nucl. Instrum. Meth. Phys. Res. A* **278** 38 (1989)
51. Nardi E, Peleg E, Zinamon Z *Phys. Fluids* **21** 574 (1978)
52. Larkin A I *Zh. Eksp. Teor. Fiz.* **37** 264 (1959) [*Sov. Phys. JETP* **10** 186 (1960)]
53. Hoffmann D H H et al. *Phys. Rev. A* **42** 2313 (1990)
54. Dietrich K-G et al. *Laser Part. Beams* **8** 583 (1990)
55. Dietrich K-G et al. *Z. Phys. D* **16** 229 (1990)
56. Dietrich K-G et al. *Phys. Rev. Lett.* **69** 3623 (1992)
57. Wetzler H et al. *Laser Part. Beams* **15** 449 (1997)
58. Betz H-D *Rev. Mod. Phys.* **44** 465 (1972)
59. Jacoby J et al. "Stopping of heavy ions in a hydrogen plasma" *Phys. Rev. Lett.* **74** 1550 (1995)
60. Kowalewicz R et al. *Laser Part. Beams* **14** 599 (1995)
61. Belyaev G et al. *Phys. Rev. E* **53** 2701 (1996)
62. Golubev A et al. "Dense plasma diagnostics by fast proton beams" *Phys. Rev. E* **57** 3363 (1998)
63. Golubev A et al. "Experimental investigation of the effective charge state of ions in beam-plasma interaction" *Nucl. Instrum. Meth. Phys. Res. A* **464** 247 (2001)
64. Golubev A et al. "Experimental investigation of the effective charge state of ions in beam-plasma interaction", Annual Report GSI-99-04 (1999) p. 6
65. Kulish M et al. "Dynamic plasma pressure measurements" *Rev. Sci. Instrum.* **72** 2294 (2001)
66. Ziegler J F *Nucl. Instrum. Meth. Phys. Res. B* **219–220** 1027 (2004); SRIM-2000, SRIM-2003, http://www.srim.org/
67. Servajean A et al. *J. Appl. Phys.* **71** 2587 (1992)
68. Gardes D et al. *Phys. Rev. A* **46** 5101 (1992)
69. Chabot M et al. *Phys. Rev. E* **51** 3504 (1995)
70. Chabot M, Gardes D, Kiener J *Laser Part. Beams* **13** 293 (1995)
71. Chabot M et al. *Nucl. Instrum. Meth. Phys. Res. B* **415** 571 (1998)
72. Roth M et al. "Energy loss of heavy ions in laser-produced plasmas" *Europhys. Lett.* **50** 28 (2000)
73. Sakumi A et al. *Nucl. Instrum. Meth. Phys. Res. A* **464** 231 (2001)
74. Oguri Y et al. *Nucl. Instrum. Meth. Phys. Res. A* **415** 657 (1998)
75. Shibata K et al. *Nucl. Instrum. Meth. Phys. Res. A* **464** 225 (2001)
76. Gericke D O, Schlanges M *Phys. Rev. E* **60** 904 (1999)
77. Zwicknagel G, Toepffer C, Reinhard P-G *Phys. Rep.* **309** 117 (1999); *Laser Part. Beams* **13** 311 (1995)
78. Mintsev V et al. "On measurements of stopping power in explosively driven plasma targets" *Nucl. Instrum. Meth. Phys. Res. A* **415** 715 (1998)
79. Mintsev V et al. "Stopping power of proton beam in a weakly non-ideal xenon plasma" *Contrib. Plasma Phys.* **39** 45 (1999)
80. Weyrich K et al. "First Energy Loss Measurements in Shockwave-driven, Non-ideal Plasmas, in HED Matter Produced by Heavy Ion Beams", Annual Report 2001, GSI-2002-7 Report Nov. 2001
81. Weyrich K et al. "Shockwave-driven, non-ideal plasmas for interaction experiments with heavy-ion beams" *J. Phys. A: Math. Gen.* **39** 4749 (2006)

82. Dornik M et al. "Heavy-ion-beam-induced motion in rare-gas cryo targets" *Fusion Eng. Design* **32 – 33** 511 (1996)

83. Stöwe S et al. "Heavy-ion-induced hydrodynamic motion in lead targets" *Laser Part. Beams* **18** 573 (2000)

84. Roudskoy I V et al. "Gamma radiation measurements as a diagnostic tool of beam-induced dense plasmas" *Laser Part. Beams* **23** 539 (2005)

85. Varentsov D et al., Scientific Report 2003, GSI-Darmstadt, GSI-2004-01 (2004) p. 137

86. Ni P et al. "Pyrometric system for temperature measurements of HED matter generated by intense heavy ion beams" *J. Phys. IV* (France) **133** 977 (2006)

87. Golubev A et al. "Diagnostics of plasma target for ion beam: target interaction experiments" *Fusion Eng. Design* **32 – 33** 557 (1996)

88. Varentsov D et al. *Laser Part. Beams* **20** 485 (2002)

89. Bushman A V et al. *Intense Dynamic Loading of Condensed Matter* (London: Taylor & Francis, 1992)

90. Kanel G I et al. *J. Appl. Phys.* **79** 8310 (1996)

91. Levin J, Tzach D, Shamir J *Rev. Sci. Instrum.* **67** 1434 (1996)

92. Weng J et al. "New all-fiber velocimeter" *Rev. Sci. Instrum.* **76** 093301 (2005)

93. Udrea S et al. "Electrical resistivity measurements of heavy ion beam generated high energy density aluminium" *J. Phys. A: Math. Gen.* **39** 4743 (2006)

94. Duderstadt J J, Moses G A *Inertial Confinement Fusion* (New York: Wiley, 1982) [Translated into Russian (Moscow: Energoatomizdat, 1984)]

95. Hogan W J (Ed.) *Energy from Inertial Fusion* (Vienna: IAEA, 1995)

96. Mima K et al., in *Inertial Fusion Science and Application 99* (Eds C Labaune, W Hogan, K Tanaka) (Amsterdam: Elsevier, 2000) p. 381

97. Bock R "Inertialfusion mit Schwerionenstralen", Preprint GSI 2001-32

98. Sharkov B Yu (Ed.) *Yadernyi Sintez s Inertsionnym Uderzhaniem — Sovremennoe Sostoyanie i Perspektivy dlya Energetiki* (Inertial Confinement Fusion — Current State and Prospects for Energy Production) (Moscow: Fizmatlit, 2005)

99. Pellat R "Ignition: a dual challenge", in *Inertial Fusion Science and Application 99* (Eds C Labaune, W Hogan, K Tanaka) (Amsterdam: Elsevier, 2000) p. 3

100. Koshkarev D G, Churazov M D "Inertsionnyi termoyadernyi sintez na baze tyazheloionnogo uskoritelya-draivera i tsilindricheskoi misheni" *At. Energ.* **91** (1) 47 (2001) ["Inertial confinement fusion with a heavy-ion driver-accelerator and cylindrical target" *At. Energy* **91** 564 (2001)]

101. Koshkarev D G "Charge-symmetric driver for heavy-ion fusion" *Nuovo Cimento A* **106** 1567 (1993)

102. Hofmann I, Plass G (Eds) "The HIDIF Study", GSI Report 98-06 (1998); Hofmann I *Nucl. Instrum. Meth. Phys. Res. A* **415** 11 (1998)

103. Logan B G *Laser Part. Beams* **20** 369 (2002)

104. Barnard J J et al. "Induction accelerator architectures for heavy-ion fusion" *Nucl. Instrum. Meth. Phys. Res. A* **415** 218 (1998)

105. Lindl J D *Inertial Confinement Fusion* (New York: Springer, 1998)

106. Yu S et al. "Plasma-channel-based reactor and final transport" *Nucl. Instrum. Meth. Phys. Res. A* **415** 174 (1998)

107. Tauschwitz A et al., in *Inertial Fusion Science and Application 99* (Eds C Labaune, W Hogan, K Tanaka) (Amsterdam: Elsevier, 2000) p. 521

108. Sharkov B Yu "Heavy-ion fusion activities at ITEP" *Nucl. Instrum. Meth. Phys. Res. A* **415** 20 (1998)

109. Friedman A et al. *Nucl. Instrum. Meth. Phys. Res. A* **464** 653 (2001)

110. Haber I et al. *Nucl. Instrum. Meth. Phys. Res. A* **415** 405 (2001)

111. Basko M M, Churazov M D, Koshkarev D G *Fusion Eng. Design* **32 – 33** 73 (1996)

112. Vatulin V V et al. *Fusion Eng. Design* **32 – 33** 609 (1996)

113. Basko M M, Churazov M D, Aksenov A G *Laser Part. Beams* **20** 411 (2002)

114. Tabak M et al. *Nucl. Fusion* **38** 509 (1998)

115. Callahan-Miller D A, Tabak M *Phys. Plasmas* **7** 2083 (2000)

116. Basov N G, Gus'kov S Yu, Feoktistov L P *J. Sov. Laser Res.* **13** 396 (1992)

117. Tabak M et al. *Phys. Plasmas* **1** 1626 (1994)

118. Moir R W "Liquid wall inertial fusion energy power plants" *Fusion Eng. Design* **32 – 33** 93 (1996)

119. Badger B et al. "HIBALL-II — An improved conceptual heavy beam driven fusion reactor study", Report KfK No. 3840 (Karlsruhe: Kernforschungszentrum, 1984)

120. Bourque R F, Meier W R, Mousler M J "Overview of the Osiris IFE reactor conceptual design" *Fusion Technol.* **21** 1465 (1992)

121. Meier W R, Wagaver L M "Recent heavy-ion fusion power plant studies in the US" *Nuovo Cimento A* **106** 1983 (1993)

122. Medin S A *Laser Part. Beams* **20** 419 (2002)

123. Medin S et al. "Osnovnye parametry energeticheskoi ustanovki na osnove tyazheloionnogo termoyadernogo sinteza v kontseptsii bystrogo podzhiga" ("Main parameters of heavy ion fusion power plant with fast ignition"), Preprint (Moscow: ITEP, 2002)

124. Sharkov B "Status of heavy ion fusion" *Plasma Phys. Control. Fusion* **43** A229 (2001)

125. Suit H "The Gray lecture 2001: coming technical advances in radiation oncology" *Int. J. Radiat. Oncol. Biol. Phys.* **53** 798 (2002)

126. Suit H "Gray Lecture 2001 (Greevskaya lektsiya 2001): Gryadushchie tekhnicheskie dostizheniya v radioonkologii" *Med. Fiz.* (1) 66 (2005)

127. Khoroshkov V S, Minakova Ye I "Proton beams in radiotherapy" *Eur. J. Phys.* **19** 523 (1998)

128. Khoroshkov V S "Evolyutsiya tekhnologii luchevoi terapii: ot rentgena k adronam" *Yad. Fiz.* **69** 1760 (2006) ["Radiation beam therapy evolution: from X-rays to hadrons" *Phys. At. Nucl.* **69** 1724 (2006)]

129. Kraft G "Tumor therapy with heavy charged particles" *Prog. Part. Nucl. Phys.* **45** (Suppl. 2) S473 (2000)

130. Amaldi U, Kraft G "Recent application of synchrotrons in cancer therapy with carbon ions" *Europhys. News* 114 (2005)

131. Klenov G I, Khoroshkov V S "Razvitie protonnoi luchevoi terapii v mire i v Rossii. Ch. 1" ("Progress in proton therapy in Russia and the world. Pt. 1") *Med. Fiz.* (3) 16 (2005)

132. Klenov G I, Khoroshkov V S "Razvitie protonnoi luchevoi terapii v mire i v Rossii. Ch. 2" ("Progress in proton therapy in Russia and the world. Pt. 2") *Med. Fiz.* (4) 9 (2005)